M 2023

U.PORTO
FEUP FACULDADE DE ENGENHARIA
UNIVERSIDADE DO PORTO

EXPERIMENTAL TESTING ON TUNED LIQUID DAMPERS (TLD) AIMING THEIR IMPLEMENTATION ON INDUSTRUAL CHIMNEYS

GIANCARLO BADINI MARULLI
DISSERTAÇÃO DE MESTRADO APRESENTADA
À FACULDADE DE ENGENHARIA DA UNIVERSIDADE DO PORTO EM
ENGENHARIA CIVIL - ESPECIALIZAÇÃO EM ESTRUTURAS E GEOTECNIA

Experimental testing on Tuned Liquid Dampers (TLD) aiming their implementation on industrial chimneys

Giancarlo Badini Marulli

Dissertação submetida para satisfação parcial dos requisitos do grau de

Mestre em Engenharia Civil — Especialização em Estruturas e Geotecnia

Orientador: Professor Doutor Carlos Manuel Ramos Moutinho

junho de 2023

MESTRADO EM ENGENHARIA CIVIL 2021/2022

DEPARTAMENTO DE ENGENHARIA CIVIL

Tel. +351-22-508 1901

 m.ec@fe.up.pt

Editado por

FACULDADE DE ENGENHARIA DA UNIVERSIDADE DO PORTO

Rua Dr. Roberto Frias

4200-465 PORTO

Portugal

Tel. +351-22-508 1400

 feup@fe.up.pt

 http://www.fe.up.pt

Ao povo português.

"Os muros das construções são o papel onde se inscreveram as páginas da história, onde ainda se inscrevem as mensagens para o futuro."

Joaquim Cardozo

Agradecimentos

Gostaria de agradecer, primeiramente, ao meu orientador, prof. dr. Carlos Moutinho, por ter me dado a oportunidade de o acompanhar em atividades da engenharia desde o meu segundo ano de curso, que culminaram na idealização e na realização desta dissertação, e por ter sido um excelente orientador.

Agradeço também ao sr. Philippe Duflot por ter possibilitado a realização deste trabalho em associação com sua empresa e por todo o conhecimento que partilhou comigo no seu decorrer.

Deixo meus agradecimentos aos funcionários do Laboratório de Estruturas da FEUP: Guilherme, Cláudio, Nuno e Paula, pela ajuda técnica e por terem sido sempre atenciosos durante minha estadia no laboratório; e ao prof. Alexandre Pinto por ter me emprestado o reservatório que utilizei na realização dos experimentos.

Por fim, não posso deixar de agradecer meus pais, Enzo e Kathia, e ao meu irmão e sua esposa, Enrico e Claudia. Não existem palavras nesse mundo capazes de descrever todo o apoio que eles me deram ao longo da minha vida.

Acknowledgements

First, I would like to thank my supervisor, prof. dr. Carlos Moutinho, for allowing me to accompany him in engineering activities since my second year at the course, which led to the idealisation and accomplishment of this thesis, and for being an excellent supervisor.

I also thank to mr. Philippe Duflot for allowing the making of this study in association with his company and for all the knowledge he shared with me during its execution.

I express gratitude to all the employees of the Laboratory of Structures of FEUP: Guilherme, Cláudio, Nuno e Paula, for the technical support and for always being polite while I stayed in the lab; and also to prof. Alexandre Pinto for lending me the reservoir that I used in this study's tests.

Lastly, I thank my parents, Enzo and Kathia, and my brother and his wife, Enrico and Claudia. There are no words that could express how much they supported me through all my life.

ABSTRACT

This study was developed as the author's master’s thesis in Civil Engineering in the Faculty of Engineering of the University of Porto (FEUP) in collaboration with Modalyse Engineering. The annular TLD in study was designed to be installed in the steel chimneys of a heat recovery steam generator at Toplarna Power Plant in Ljubljana, Slovenia.

Chimneys have been used as a way to conduct and disperse fumes and other undesirable gases since Antiquity. Being tall and slender structures with low damping coefficients, they are vulnerable to significant vibrations mainly caused by the wind.

A TLD is a passive damping device whose core mechanism at work is the dissipation of energy due to the sloshing of the liquid and the effect of wave breaking, therefore controlling the vibrations of the structure. When associated with the structure, a TLD creates a two mass system. This lowers the amplitude of the structure’s vibrations when the acting excitation is in resonance with it, which is very useful as this amplitude is maximum under resonance.

The main objective of this study is to evaluate the behaviour of an annular TLD composed of multiple cells through laborital tests. It will be analysed if it is reasonable to design it as an agglomeration of smaller rectangular TLD and the influence of the amplitude of displacement in the behaviour of the annular TLD will also be in analysis.

The tests were performed with a shaking table and two pendulums of same length but of different masses. Three reservoirs were studied as TLD: a rectangular one, one built like a cell of the annular TLD and one built like a quarter-ring of the annular TLD due to spatial limitations.

This study reached the conclusion that the analytical methods developed in previous studies were in general adequate for the design of a rectangular TLD and that it was reasonable to design the annular TLD studied as a combination of rectangular ones, as its cells were a close match to a rectangle of similar dimensions. It also reached the conclusion that a compartmentalised annular TLD is an adequate solution for the vibration control of structures with high displacements.

KEYWORDS: TUNED MASS DAMPER, TLD, ANNULAR TLD, PASSIVE DAMPING, VIBRATION CONTROL

RESUMO

Este estudo foi desenvolvido como a tese de mestrado em Engenharia Civil do autor na Faculdade de Engenharia da Universidade do Porto (FEUP) em colaboração com a empresa Modalyse Engineering. O TLD anelar em estudo foi desenvolvido para ser instalado numa chaminé industrial de uma caldeira de recuperação no complexo elétrico de Toplarna em Liubliana, Eslovénia.

Chaminés foram usadas como condutores e dispersores de fumos e outros gases indesejados desde a Antiguidade. Sendo estruturas altas e esbeltas, com baixos coeficientes de amortecimento, elas são vulneráveis a ações dinâmicas, principalmente as causadas pelo vento.

Um TLD é um dispositivo de amortecimento passivo cujo mecanismo de funcionamento é a dissipação de energia pelo movimento do líquido e pelo efeito de quebra de ondas controlando, assim, as vibrações da estrutura. Quando associado a uma estrutura, o TLD cria um sistema de duas massas que resulta numa redução da amplitude de deslocamentos da mesma em sua ressonância, o que é muito útil, uma vez que os maiores deslocamentos ocorrem nessa situação.

O principal objetivo do trabalho é avaliar o comportamento de um TLD anelar composto por múltiplas células através de testes laboratoriais. Será determinado se é razoável projetar esse tipo de TLD como um aglomerado de pequenos TLD retangulares. A influência da amplitude de deslocamento no TLD anelar também será analisada.

Foram realizados testes laboratoriais com uma mesa sísmica e com dois pêndulos do mesmo comprimento, mas com massas diferentes. Três reservatórios foram estudados como TLD: um retangular, um no formato de uma das células do TLD anelar e um construído como um quarto do TLD anelar em estudo por questões de escala.

Chegou-se à conclusão de que os métodos analíticos desenvolvidos por estudos passados são em geral adequados para o dimensionamento de TLD retangulares e que seria razoável projetar um TLD anelar similar ao em estudo como sendo composto por múltiplos TLD retangulares, uma vez que cada uma das células se comporta de forma muito similar a um reservatório retangular de dimensões similares. Também foi possível concluir que um TLD anelar compartimentado é uma solução adequada para o controle de vibrações de estruturas com grandes deslocamentos.

PALAVRAS-CHAVE: AMORTECEDORES DE MASSA LÍQUIDA SINTONIZADA, TLD, TLD ANELAR, AMORTECIMENTO PASSIVO, CONTROLE DE VIBRAÇÕES

Index

List of Figures

LIST OF TABLES

Symbols, Acronyms and Abbreviations

Letters as symbols

A - amplitude of displacement [m]

b - width of a reservoir [m]

c - damping constant of a structure [ton/s]

c_{cr} - critical damping constant of a structure [ton/s]

C_{wb} - coefficient of wave breaking

f - frequency of a structure [Hz]

f_f - sloshing frequency [Hz]

f_0 - central frequency [Hz]

F - base shear force [kN]

g - acceleration of gravity [m/s²]

h_f - height of liquid/water inside the TLD [m].

k - stiffness of a structure [kN/m]

L - length [m]

M - mass [ton]

p - dynamic load [kN]

R_{ext} - external radius of a TLD [m]

S - “surface contamination” factor

t - time [s]

T - period [s]

u - displacement [m]

u_o - initial displacement of the structure [m]

u' - velocity [m/s]

u'_o - initial velocity of the structure [m/s]

u'' - acceleration [m/s²]

Greek letters as symbols

β - frequency spacing [Hz]

γ - specific weight [kN/m³]

ε - liquid depth ratio

ε_0 - central liquid depth ratio

η - maximum liquid surface elevation [m]

λ - damping constant of liquid motion [rad/s]

λ_{water} - damping constant of liquid motion of water [rad/s]

μ - ratio of masses

ν - kinematics viscosity [m²/s]

ξ - damping coefficient

ξ_{nm} - root of the transcendental equations related to the Bessel functions of order n

ω - natural frequency of a structure [rad/s]

ω_d - damped natural frequency of a structure [rad/s]

ω_f - sloshing frequency [rad/s]

Multiple letters as symbols

ΔE - energy dissipated [MJ]

ΔR - frequency distribution range for MTLD

$\Delta\gamma$ - mis-tuning factor for MTLD

Acronyms

TLD - Tuned Liquid Damper(s)

MTLD - Multiple Tuned Liquid Dampers

TMD - Tuned Mass Damper(s)

SDOF - Single Degree of Freedom

MDOF - Multiples Degrees of Freedom

FFT - Fast Fourier Transformation

1
INTRODUCTION

1.1: Contextualisation

This study was developed as the author's master's thesis in Civil Engineering in the Faculty of Engineering of the University of Porto (FEUP) in collaboration with Modalyse Engineering, a structural engineering office whose expertise is in structural engineering, dynamics and monitoring of structures focusing on high-performance engineering service. The experimental tests were performed in the Laboratory of the Structural Section of FEUP, under management of the Laboratory of Vibrations and Structural Monitoring (ViBest).

The annular TLD in study was designed to be installed in the steel chimneys of a heat recovery steam generator at Toplarna Power Plant in Ljubljana, Slovenia. Previous studies of this TLD configuration have been conducted by Modalyse (some in conjunction with FEUP), but further experimentation is still required, which is the aim of this study.

Figure 1.1 - Toplarna Power Plant. [Open House Slovenia]

1.2: Structures and vibration control devices

Chimneys have been used as a way to conduct and disperse fumes and other undesirable gases since Antiquity. Being tall and slender structures with low damping coefficients, they are vulnerable to dynamic forces mainly caused by the wind. As pointed out by Gala (2013), Jorge (2017) and many others, the wind is particularly prejudicial to chimneys due to the formation of a vortex shedding effect caused by the wind breaking when flowing around the chimney, which causes the structure to vibrate.

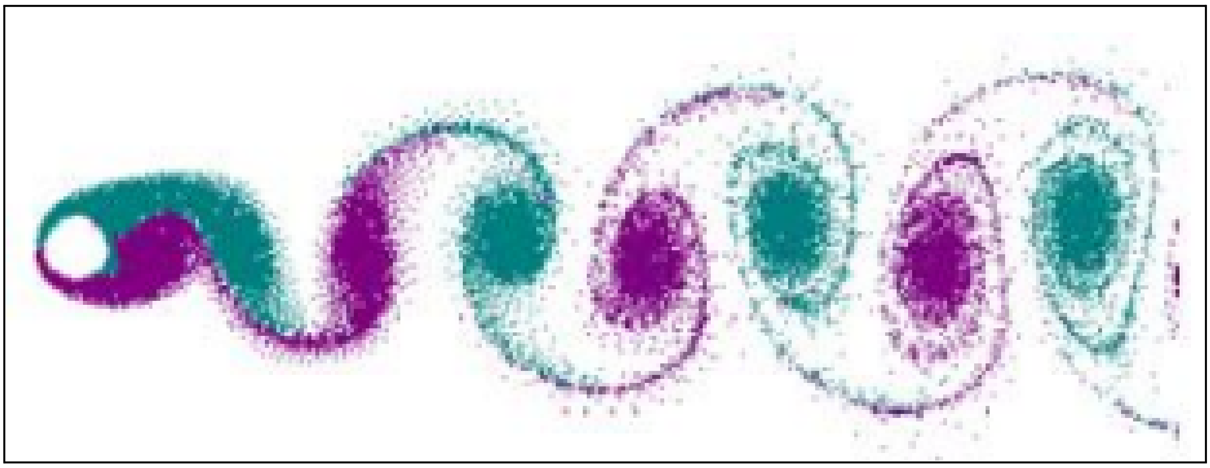

Figure 1.2 - Vortex shedding on a cylinder [Jorge, 2017]

As is well established, dynamic actions (such as earthquakes or the wind) can induce vibrations in a structure that may lead to degradation, loss of stability and even to failure. As pointed out by Moutinho (1998), even when the level of vibration detected in the structure is not severe enough to put its integrity into jeopardy they may lead to discomfort to part of the occupants of the building.

“In this case, the introduction of vibration control systems with the intent to reduce the level of vibration detected to an acceptable one is justified, looking at it from a structural point of view and also from a human comfort one.” [Moutinho, 1998]

These systems are usually created through the introduction of a damping device in the structure. These devices are usually designed to control the first mode of vibration as it tends to be the most relevant in general structures that have multiple degrees of freedom, as pointed out by Konar & Gosh (2022).

“As normal civil engineering structures such as buildings, pylons of bridges, and chimneys have maximum displacement near their top under the first mode of vibration, inertia-based dampers are normally placed near the top of the structure. However, sometimes multimodal vibration control is also attempted using vibration control devices.” [Konar & Ghosh, 2022]

In this study, the damping device of choice is the Tuned Liquid Damper. Tuned Liquid Dampers (or TLD) are a kind of passive damping device that evolved from the more conventional Tuned Mass Dampers (or TMD), sharing some of their properties with them. According to Jamal (2015), TLD were initially developed for utilisation in Aerospace and Marine Engineering in the beginning of the 20th century. However, their application in Civil Engineering started to be studied only in the mid 1980s. Modi and Welt were pioneers in this field, analysing the implementation of nutational TLD (annular and toroidal), similar to those present in satellites, in buildings.

In the time between their study and this one, more research was done in the area, such as the ones conducted by Sun (1991), Fujino et al. (1992), Soong & Spencer (2002), Ramos (2010), Novo et al. (2014), Jamal (2015), Ghaemmaghami et al. (2016), Yue et al. (2018), Konar & Gosh (2022), among many others.

This led to the popularisation of TLD applications in Civil Engineering in the last decades, due to them being easy to implement, simple to understand on a basic level and requiring a small investment and maintenance when compared to other damping systems.

Although some of the newer studies focused on the design and application of TLD of different shapes, most research done still focuses on rectangular and circular designs. This is one of the problems this study is meant to tackle. But first, there is some base information that should be convened.

1.3: A brief overview of passive damping devices

A passive damping device is a damper that does not require any external energy supply to operate. To be effective, these devices must be designed taking into account the structure onto which they are going to be installed.

“This kind of technique has been widely implemented in Civil Engineering structures with particular emphasis in the area of Earth-quake Engineering. Most passive devices are prepared to deal with forces of high amplitude and have high capacity for dissipation of energy. Furthermore, compared with other techniques, passive control is more interesting in terms of reliability, cost and maintenance. For these reasons, in the process of studying a system to reduce vibrations in a structure, passive control should be considered as the first solution, and just in case this is not effective enough, move to other more sophisticated techniques. As its main disadvantage, passive systems are generally less efficient than active systems, particularly in situations that require some adaptability of the control force depending on the structural response.” [Moutinho et al., 2010]

Both TMD and TLD are passive devices, their main difference conceptually is that the former is composed of a solid mass while the latter is composed of a liquid mass.

1.3.1: Tuned Mass Damper (TMD)

Before moving on to the TLD, it is useful to study, even if just briefly, the operation principle of a TMD. As mentioned before, they operate in a similar fashion.

As Soong & Spencer (2002) pointed out, TMD started being used in Civil Engineering as a way to control the vibrations induced by wind on structures. By the time of his studie, TMD were already being used to control seismic responses as well. He also pointed out that: “[...] a passive TMD can only be tuned to a single structural frequency. While the first-mode response of a MDOF structure with TMD can be substantially reduced, the higher mode response may in fact increase as the number of stories increases. For earthquake-type excitations, the response reduction is large for resonant ground motions and diminishes as the dominant frequency of the ground motion gets further away from the structure's natural frequency to which the TMD is tuned." [Soong & Spencer, 2002]

"A TMD is generally composed by an additional mass fixed to the structure through the association of a spring and a damping device in parallel, acting as a single degree of freedom system whose natural frequency is slightly below that of the natural frequency of the structure. The control's action is exerted by the joint reaction of the spring and the damper onto the main structure; this is a function of time and acts in the opposite directions of the movement of the structure." [Moutinho, 1998]

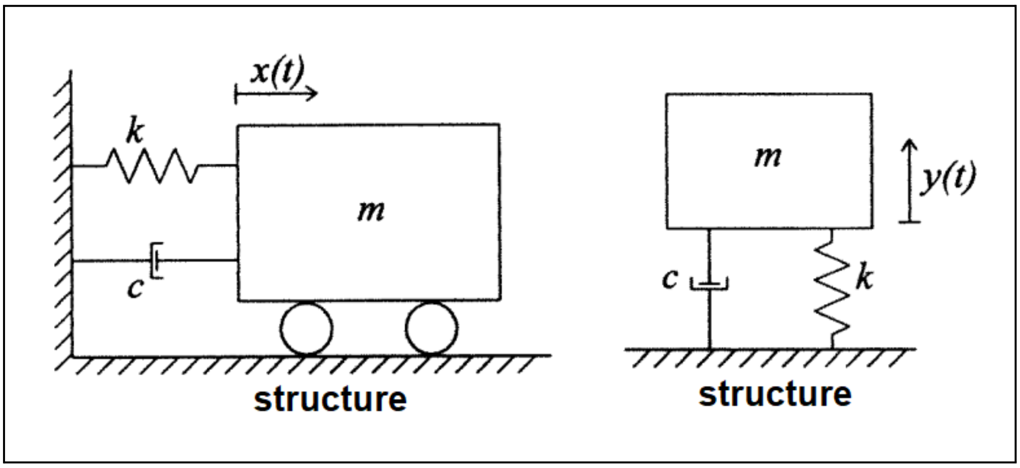

Figure 1.3 - Schematic representation of a TMD. [Moutinho, 1998]

As is pointed out by Moutinho (1998), when a TMD is installed in a previously undamped structure, the behaviour of the system changes. Instead of having one peak of displacement when the acting excitation is in resonance with the system (in the natural frequency of the structure), two peaks will be noticed. These peaks will be smaller than the original one and will be developed in frequencies that flank the natural frequency of the structure; the distance in which they occur depends on the magnitude of the damper coefficient.

1.3.2: Tuned Liquid Damper (TLD)

A typical TLD is a rectangular reservoir filled with liquid, usually water, to a certain level. The core mechanism at work is the dissipation of energy due to the sloshing of the liquid and the effect of wave breaking, therefore controlling the vibrations of the structure.

"The basic principles involved in applying a tuned liquid damper (TLD) to reduce the dynamic response of structures is quite similar to that [...] for the TMD. In effect, a secondary mass in the form of a body of liquid is introduced into the structural system and tuned to act as a dynamic vibration absorber. However, in the case of TLD, the damper response is highly nonlinear due either to liquid sloshing or the presence of orifices. TLD have also been used for suppressing wind-induced vibrations of tall structures.” [Soong & Spencer, 2002]

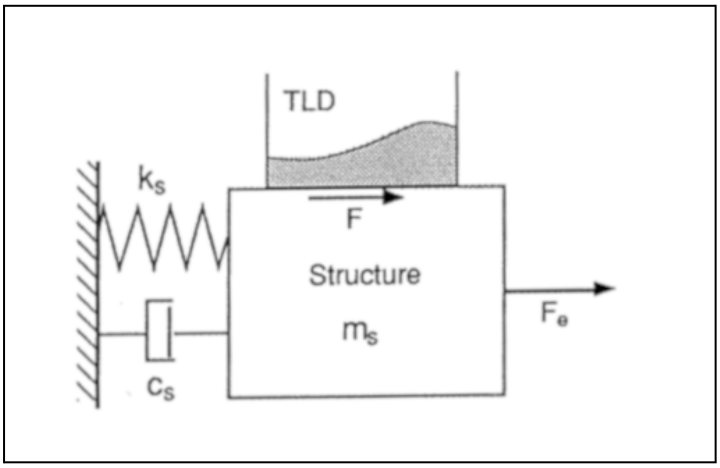

Figure 1.4 - TLD-structure interaction under horizontal motion. [Sun, 1991]

This is corroborated by Ramos (2010) as well as by others. Ramos also pointed out the importance of the deformation of the liquid mass and its interactions with the lateral walls of the reservoir as one of the causes of the difference in behaviour between the TLD and the TMD.

“However, in reality, the liquid interaction with the reservoir walls can be quite complex and a simple SDOF analogy is an improper simplification in most applications. This is the key factor which differentiates TLD design from that of a TMD. Nevertheless, TLD have a near-zero acceleration trigger level, which makes them very attractive for damping horizontal structural sway with very low frequencies and displacements. Also, water-filled reservoirs are quite cheap and easy to maintain, hence TLD are inexpensive solutions, and definitely worth exploring.” [Ramos 2010]

As is the case with TMD, TLD associated to the structure create a two mass system. In both cases, the natural frequency of vibration of the device is tuned to the structure’s one, but with a 90º phase angle between them. This lowers the amplitude of the structure’s vibrations when the acting excitation is in resonance with it, which is very useful as this amplitude is maximum under resonance.

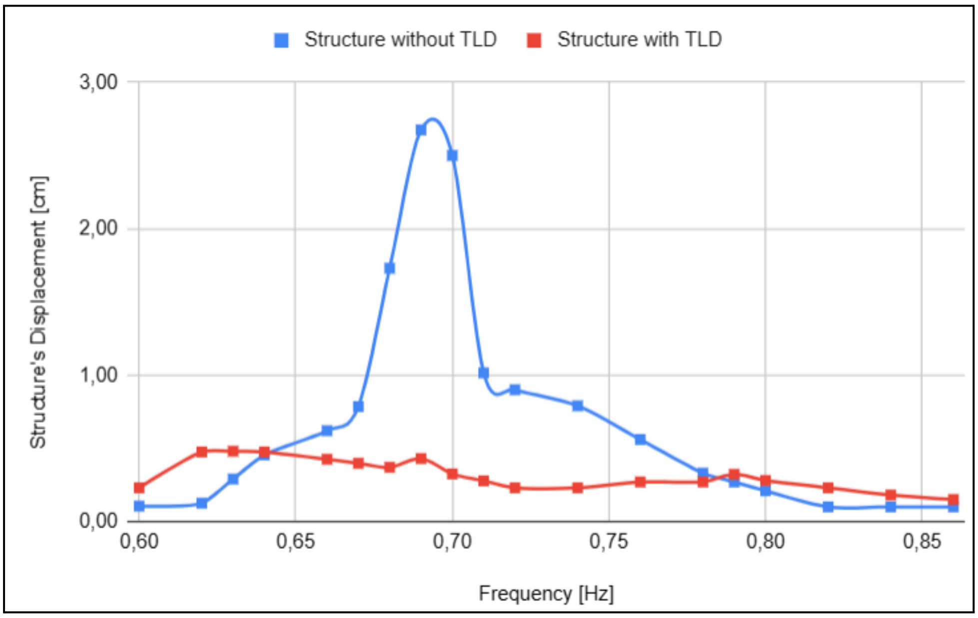

Figure 1.5 - Frequency-response curve of a structure before and after a TLD is installed.

1.4: Objectives

The main objective of this study is to evaluate the behaviour of an annular TLD composed of multiple cells through laborital tests. It will be analysed if it is reasonable to design it as an agglomeration of smaller rectangular TLD disposed around a circumference with different angles to the acting excitation and its applicability in the control of vibrations in industrial chimneys. The influence of the amplitude of displacement in the behaviour of the ring TLD will also be in analysis.

As a necessity for the main goal, tests to evaluate if the current analytical formulas used on the design of rectangular TLD will be made, focusing on the influence of the liquid height and reservoir length on the performance of the TLD.

The influence of the input direction on performance of a rectangular TLD will also be evaluated before finally transitioning from the rectangular reservoir to a annular TLD composed of several quasi-rectangular cells where the knowledge accumulated in the previous tests will be applied to further this study's main goal.

1.5: Expected results

Due to the extensive research performed with the rectangular TLD, it is expected that the results from the experimental tests will be a close match to the ones predicted through the analytical methods in use. The behaviour of the liquid when the reservoir is not aligned with the movement is still unknown, but it is expected that there will be great amounts of interference as the waves break against the corners of the reservoir and also that the performance of the TLD will decrease the more the reservoir is rotated.

It is expected that the behaviour of each cell of the annular TLD will be a close match to that of a rectangular one, if only a little less effective due to the cell's geometry not being taken totally into account when tuning them to the structure. As is the case with the regular TLD, a reduction in the contribution of the cells that are not aligned to the introduced excitation is expected, as the waves in these cells are expected to break due to the corners of the reservoir.

As for the annular TLD, it is expected that its behaviour will be more similar to an agglomeration of rectangular reservoir than to that of a conventional annular TLD due to it being divided into quasi-rectangular cells.

2
STATE OF THE ART

2.1: Introduction

Dynamic actions are those actions whose magnitude, direction and/or point of application vary in time; therefore, a structure's response to a dynamic load, also varies in time. Examples of dynamic loads in structures include: earthquakes, the effect of an operating machine, the effect of a group walking and, more relevant to the present study, the wind. The wind acts on a structure as a periodic load.

"[...] periodic loadings are repetitive loads which exhibit the same time variation successively for a large number of cycles. The simplest periodic loading is the sinusoidal variation [...], by the means of a Fourier analysis, any periodic loading can be represented as the sum of a series of simple harmonic components; thus, in principle, the analysis of response to any periodic loading follows the same general procedure." [Clough, 1975]

The response of a single degree of freedom structure to a dynamic load can be expressed by its equation of motion, the structural dynamic's fundamental equation:

$$m \times u''(t) + c \times u'(t) + k \times u(t) = p(t) \tag{1}$$

with: m being the mass of the structure [ton]; c being the damping constant of the structure [ton/s]; k being the stiffness of the structure [kN/m]; $p(t)$ being the dynamic load [kN]; $u(t)$ being the displacement of the structure in an instant t [m], with $u'(t)$ and $u''(t)$ being its first and second-order derivatives with respect to time (the structure's velocity [m/s] and acceleration [m/s^2], respectively); and t being the time [s].

Each group of terms of the equation of motion equates to a different kind of force in the system. The first group (mass and acceleration) corresponds to the force of inertia, the second one (damping and velocity) to the damping force, and the third one (stiffness and displacement) to the elastic force.

When a structure is subjected to an periodic load its response can be divided in two components. The first one is the transient state response and the second is the steady state response. In this work the response of interest is the steady state, as the transient response is in effect for a small period of time and is, therefore, not really relevant in the case of response control.

The aforementioned parameters are not the only physical quantities of interest when dealing with dynamic problems. In the case of a periodic load, the load will have an excitation frequency. Each structure also has an associated frequency, called its natural frequency, that depends on their intrinsic qualities. The natural frequency of a regular structure can be determined through the following expression:

$$f = \frac{(k/m)^{1/2}}{2 \times \pi} \tag{2}$$

with: f being the natural frequency of the structure [Hz]; m being the mass of the structure [ton]; and k being the stiffness of the structure [kN/m].

When the excitation frequency is the same as the natural frequency of the structure the system is in resonance. This is the worst case scenario, as the structural response is maximised in this case. This is clearly noticeable in a frequency curve graph, such as the one shown in Figure 2.1.

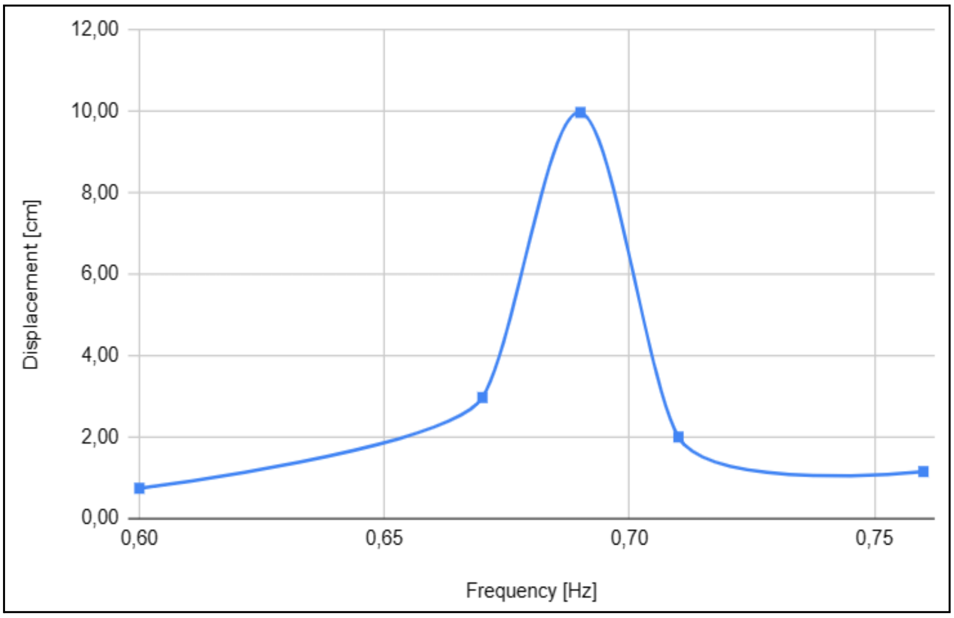

Figure 2.1 - Example of a frequency curve graph.

The frequency represents the number of cycles that occurs in an interval of time, this interval of time is deemed period. In numeric terms, the period is nothing more than the inverse of the frequency.

$$T = \frac{1}{f} \tag{3}$$

with: T being the period of excitation [s]; and f being the natural frequency of the structure [Hz].

In damped systems there is also the condition of critical damping. When a structure is critically damped, it does not develop an oscillatory movement in free vibration. The critical damping of a structure can be determined through Equation 4.

$$c_{cr} = 2 \times \sqrt{k \times m} \tag{4}$$

with: c_{cr} being the critical damping constant of the structure [ton/s]; m being the mass of the structure [ton]; and k being the stiffness of the structure [kN/m].

The damping of usual structures is a lot smaller than the critical damping. When dealing with this kind of dynamic problems, the damping is usually presented as a ratio of the structure's damping constant and its critical damping constant. This results in an adimensional parameter called damping coefficient.

$$\xi = \frac{c}{c_{cr}} \tag{5}$$

with: ξ being the damping coefficient; c being the damping constant of the structure [ton/s]; c_{cr} being the critical damping constant of the structure [ton/s].

The damping impact the natural frequency of a structure, as can be seen in Equation 6.

$$\omega_d = \omega \times \sqrt{1 - \xi^2} \tag{6}$$

with: ω_d being the damped natural frequency of the structure [rad/s]; ω being the natural frequency of the structure [rad/s]; and ξ being the damping coefficient.

These parameters are used to calculate the steady state response of a structure in free vibration through Equation 7.

$$u(t) = e^{-\xi \times \omega \times t} \times [u_o \times cos(\omega_d \times t) + \frac{u'_o + u_o \times \xi \times \omega}{\omega_d} \times sen(\omega_d \times t)] \quad (7)$$

with: $u(t)$ being the displacement of the structure in an instant t [m]; t being the time [s]; ξ being the damping coefficient; ω being the natural frequency of the structure [rad/s]; ω_d being the damped natural frequency of the structure [rad/s]; and u_o and u'_o being the initial conditions of the system (the structure's initial position [m] and velocity [m/s], respectively).

2.2: Previous works and complementary information

2.2.1: Pendulum mechanics

In this study, a pendulum was used to create an oscillatory frequency that will be used as the structure's natural frequency to which the natural frequency of the TLD (also known as sloshing frequency) will be tuned.

Pendulums have been studied since Antiquity, continuing to be in use in the Modern Era. The frequency of the pendulum depends only on its length and can be determined through Equation 8.

$$f = \frac{1}{2\times\pi} \times \sqrt{\frac{g}{L}} \quad (8)$$

with: f being the frequency of the pendulum [Hz]; g being the acceleration of gravity [m/s²]; and L being the length of the pendulum [m].

It is important to point out that the length of the pendulum cannot be too short as this would introduce vertical movements on the system that would interfere with the results. This is due to the circular trajectory of a pendulum, which means that the longer the pendulum, the greater the amplitude of movement allowed before the vertical component becomes significant.

2.2.2: Liquid sloshing behaviour

"Although the construction of a TLD is simple, the liquid sloshing motion inside the TLD is usually highly nonlinear and complex in nature. The amplitude of the sloshing motion depends on many factors such as the applied external excitation, the geometry of the tank, the depth of the liquid layer, and the properties of the contained liquid." [Ghaemmaghami et al., 2016]

As is noted by Ramos (2010) and Konar & Gosh (2022), among others, the height of liquid inside the TLD determines not only its sloshing frequency of the liquid, but also the behaviour of said sloshing, as can be seen in Figure 2.2. There is also a variation on the linearity of the sloshing depending on the disturbance of the system, as described by Ibrahim et al. (2001).

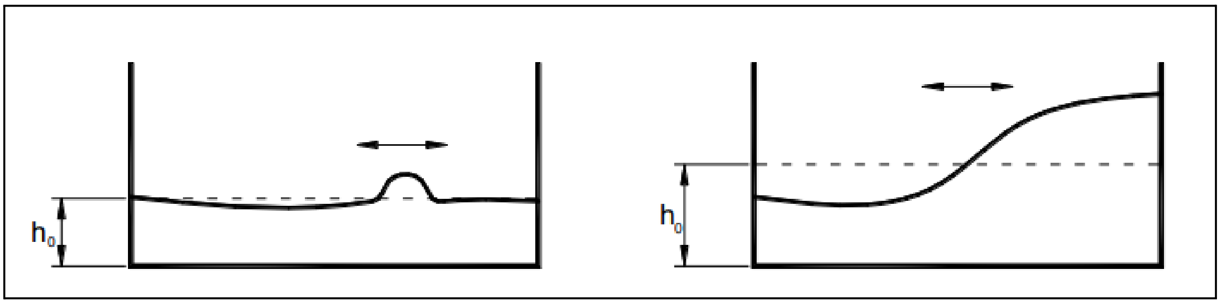

Figure 2.2 - Low (left) and high (right) fill sloshing types in rectangular containers. [Ramos 2010]

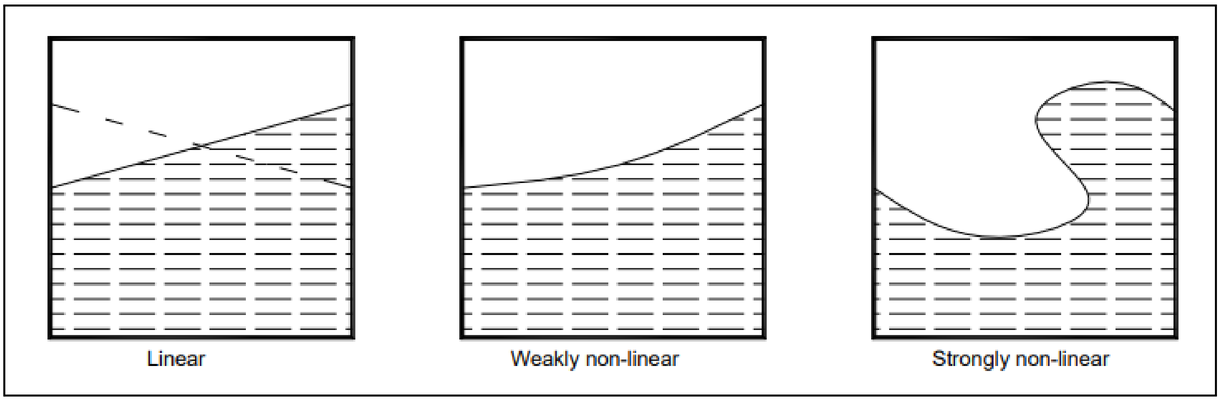

Figure 2.3 - Generic motion types in rectangular containers. [Ramos 2010]

2.2.3: Sloshing frequency

As demonstrated by Sun (1991), Fujino et al. (1992), Novo et al. (2014) and many others, the formula for the liquid sloshing frequency of the first mode of vibration is derived from the linear wave theory, developed by Lamb in 1932, and can be reliably used in the design of a rectangular TLD (Equation 9).

$$f_f = \frac{1}{2\times\pi} \times \sqrt{\frac{\pi\times g}{L} \times tanh(\frac{\pi\times h_f}{L})} \quad (9)$$

with: f_f being the sloshing frequency of the liquid (therefore of the TLD) [Hz]; g being the acceleration of gravity [m/s²]; L being the length of the TLD [m]; and h_f being the height of water inside the TLD [m].

Sun (1991) pointed out that it's impossible to tune a TLD due to the sloshing frequency dependency on the wave amplitude. This will lead to Equation 9 to result in a frequency estimation that has a 10-15% expected error. This equation is still commonly used to design TLD, but this must be taken into account. Ramos (2010) developed an equation to correct this error in sloshing frequency in small amplitude ranges through Lamb's theory. This correction will be applied if deemed necessary during the experimental phase of this study.

The analytical formula to determine the sloshing frequency of annular TLD was developed by Bauer (1960), corroborated by Ghaemmaghami et al. (2016), Yue et al. (2018) among others (Equation 10), and can be used to determine the sloshing frequency in any given mode of vibration.

$$f_f = \frac{1}{2 \times \pi} \times \sqrt{g \times \frac{\xi_{nm}}{R_{ext}} \times tanh(\frac{\xi_{nm}}{R_{ext}} \times h_f)} \quad (10)$$

with: f_f being the sloshing frequency of the liquid [Hz]; g being the acceleration of gravity [m/s²]; R_{ext} being the external radius of the TLD [m]; h_f being the height of water inside the TLD [m]; and ξ_{nm} being a root of the transcendental equations related to the Bessel functions of order n (m is just the identification number of each root).

Yue et al. (2018) pointed out that for the control of horizontal excitations the most important order of the Bessel function is the first one ($n = 1$), due to its asymmetrical behaviour in this direction. They also created a table with the values of the parameter ξ_{nm} for the different modes of sloshing. The first root of the Bessel function i.e. the value of the parameter ξ_{nm} when $m = 0$ can be used to determine the sloshing frequency of the first mode of vibration.

Table 2.1 - Excerpt from the table of values of parameter ξ_{nm} [Yue et al., 2018]

ξ_{nm}		Ratio of inner radius to outer radius — $\frac{R_{int}}{R_{ext}}$									
n	m	0	0.1	0.2	0.3	0.4	0.5	0.6	0.7	0.8	0.9
1	0	1.841	1.705	1.582	1.462	1.355	1.262	1.182	1.182	1.113	1.053
1	1	5.331	4.961	5.137	5.659	6.565	8.041	10.592	10.592	15.778	31.447
1	2	8.536	8.433	9.308	10.683	12.706	15.801	21.004	21.004	31.451	62.847

2.2.4: Damping

"Probably the simplest and most frequently used experimental method [to evaluate the damping of a single degree of freedom system] is measurement of the decay of free vibrations [...]. When a system has been set into free vibrations by any means, the damping ratio can be determined from the ratio of two displacement amplitudes measured at an interval of n cycles." [Clough, 1975]

Equation 11 can be used to estimate the damping coefficient of a system in free vibration

$$\xi = ln(\frac{u_1}{u_{n+1}})/(2 \times n \times \pi) \tag{11}$$

with: ξ being the damping coefficient; u_1 being the displacement value at the start of the free vibration; u_{n+1} being the displacement value after n cycles of the free vibration; and n being the number of cycles of the free vibration.

The effect of damping of liquid motion is significant near resonance and hence must be taken into account in the modelling of the tuned liquid damper. This can be done with Equation 12.

$$\lambda = \frac{1}{(\eta+h_f)} \times \frac{1}{\sqrt{2}} \times \sqrt{\omega \times \nu} \times (1 + \frac{2\times h_f}{b} + S) \tag{12}$$

with: λ being the damping constant of liquid motion accounting for the effect of the bottom, side wall and free surface [rad/s]; η being the maximum liquid surface elevation [m]; h_f being the height of water inside of the reservoir [m]; ω being the excitation frequency [rad/s]; ν being the kinematics viscosity of the liquid [m²/s]; b being the width of the reservoir [m]; and S being a "surface contamination" factor which accounts for damping due to stretching effect in the contaminated liquid surface.

Following in the steps of previous studies, namely Miles (1967), Lepelletier & Raichlen (1988), Sun (1991) and Fujino et al. (1992), a unitary value was taken for the surface contamination factor. Sun (1991) and Fujino et al. (1992) also found through experimentation that a more viscous liquid (namely, one that achieved $\lambda = 2.25 \times \lambda_{water}$) was better suited for damping in their particular studies.

Equation 12 does not take into consideration the effect of wave breaking when determining the damping of liquid motion. Sun (1991) empirically developed a coefficient that when multiplied by the damping of liquid motion introduces this effect in the damping of the TLD.

$$C_{wb} = 0.806 \times \sqrt{\frac{h_f^{\,2} \times \omega_f}{\nu \times b}} \times A \tag{13}$$

with: C_{wb} being the coefficient of wave breaking; h_f being the height of water inside of the reservoir [m]; ω_f being the sloshing frequency of the liquid [rad/s]; ν being the kinematics viscosity of the liquid [m²/s]; b being the width of the reservoir [m]; and A being the amplitude of the base displacement of the TLD during vibration [m].

"Although the authors have extended the theoretical model to account for breaking wave motion in rectangular TLD, it is difficult to develop a model for breaking wave motion in circular and annular TLD." [Sun, et al. 1995]

This coefficient should not be relevant for the present study, however, as the conditions of the tests were designed to avoid the wave breaking in effect.

"The effect of damping on the natural frequency is negligible if water is used as the liquid in TLD since it gives very low damping. For liquid sloshing with large wave amplitude, the resonant frequency shifts away from the natural frequency calculated due to the nonlinearity of liquid sloshing." [Sun 1991]

The damping coefficient introduced by the TLD onto the structure can be determined from the damping of liquid motion using Equation 14, as demonstrated by Sun (1991).

$$\xi = \frac{\lambda}{2 \times \omega_f} \tag{14}$$

with: ξ being the damping coefficient; λ being damping of liquid motion [rad/s]; and ω_f being the angular sloshing frequency [rad/s].

The damping coefficient of the TLD can also be determined using Equation 15, empirically developed by Abramson (1966).

$$\xi = \sqrt{\frac{\nu}{\sqrt{g \times L^3}}} \tag{15}$$

with: ξ being the damping coefficient; ν being the kinematic viscosity of the liquid [m²/s]; g being the acceleration of gravity [m/s²]; and L being the length of the TLD [m].

2.2.5: Ratio of masses

It is imperative to point out that the ratio between the masses of the damper and the structure is important as the bigger this ratio becomes, the greater is the damping provided. However, this effect has diminishing returns, so, after a certain point, the increase in mass is not viable.

As demonstrated by Warburton & Ayorinde (1980), the optimal ratio of masses for TMD is 1%, with a cutting point of around 5%. Values in this interval are usually used in the design of TMD. Most of the consulted literature utilised a ratio of masses of 1% for the TLD as well.

However, the practical experience of this study's partner company suggests that a more adequate value for the TLD would be from 5% to 10% due to the lower damping capabilities of the water.

$$\mu = \frac{M_{TLD}}{M_{str}} \tag{16}$$

with: μ being the ratio of masses; M_{TLD} being the mass of the liquid inside the TLD [kg]; and M_{str} being the mass of the structure [kg].

2.2.6: Liquid depth ratio

As demonstrated by Sim (1991), the liquid depth ratio has a great impact on the damping provided by a rectangular TLD. The higher the liquid depth ratio, the lower the damper. Furthermore, for the conditions tested in his study, it was determined that liquid depth ratio should be lower than 0.2, as this point turned out to be the cutting point, and preferably lower than 0.1. Fulfilling these last conditions drastically increased the damping coefficient.

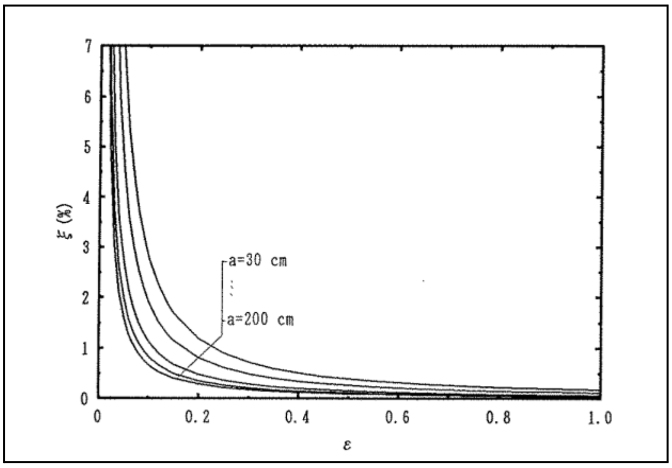

Figure 2.4 - Relation between the damping ratio and the liquid depth ratio. [Sun, 1991]

$$\varepsilon = \frac{h_f}{L/2} \tag{17}$$

with: ε being the liquid depth ratio; L being the length of the TLD [m]; and h_f being the height of water inside the TLD [m].

2.2.7: Effects of multiple rectangular TLD on a structure

The effects of multiple TLD (MTLD) on a structure started being studied in the early 1990s, Sun (1991) and Fujino & Sun (1993), were among the first to perform such studies.

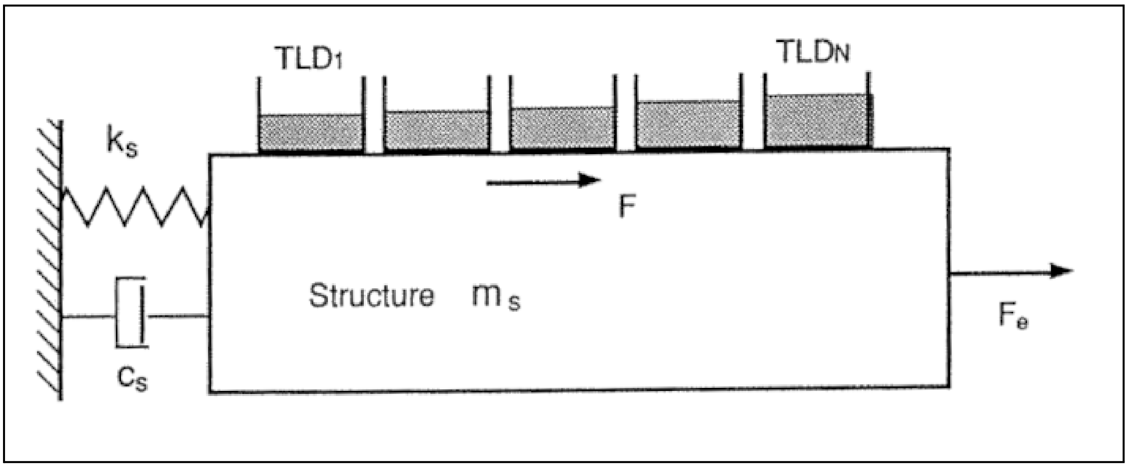

Figure 2.5 - The Multiple TLD (MTLD). [Sun, 1991]

They reached the conclusion that the most important parameters for the tuning of these systems are: the central frequency, the frequency distribution range and the frequency spacings, which are determined through Equations 18, 19 and 20, respectively.

$$f_0 = \frac{f_{max} + f_{min}}{2} \tag{18}$$

with: f_0 being the central frequency [Hz]; f_{max} being the sloshing frequency of the TLD with the highest natural frequency [Hz]; and f_{min} being the sloshing frequency of the TLD with the lowest natural frequency [Hz].

$$\Delta R = \frac{f_{max} - f_{min}}{f_0} \tag{19}$$

with: ΔR being the the frequency distribution range of the system; f_{max} being the sloshing frequency of the TLD with the highest natural frequency [Hz]; f_{min} being the sloshing frequency of the TLD with the lowest natural frequency [Hz]; and f_0 being the central frequency of the system [Hz].

$$\beta_i = f_{i+1} - f_i \tag{20}$$

with: β_i being the frequency spacing between f_i and f_{i+1} [Hz]; and with f_i and f_{i+1} being two consecutive TLD natural frequencies [Hz].

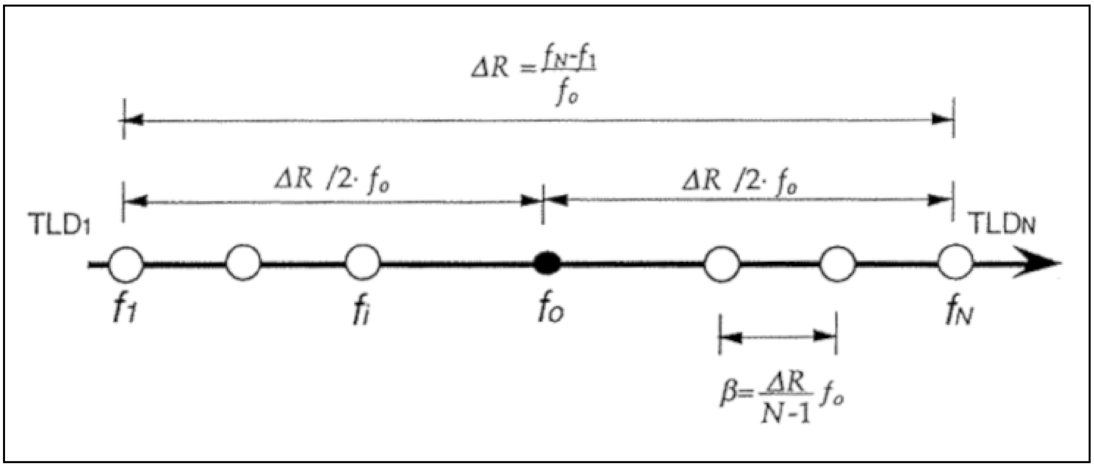

Figure 2.6 - Frequency distribution of MTLD. [Sun, 1991]

Both also studied the effect of miss-tuning in the MTLD system through the definition a a miss-tuning factor.

$$\Delta\gamma = \frac{(f - f_0)}{f_0} \tag{21}$$

with: $\Delta\gamma$ being the miss-tuning factor of the system; f being the natural frequency of the structure [Hz]; and f_0 being the central frequency of the system [Hz].

As covered by Section 2.2.6 of this study, the ratio of masses and the liquid depth ratio is important for the performance of the TLD, this remains the case with MTLD. For the ratio of masses, Equation 16 is still applicable. For the liquid depth ratio, a central value will be determined in a similar way to what was done with the sloshing frequency.

$$\varepsilon_0 = \frac{\varepsilon_{max} + \varepsilon_{minb}}{2} \tag{22}$$

with: ε_0 being the being the liquid depth ratio; ε_{max} being the being the liquid depth ratio of the TLD with the highest being the liquid depth ratio; and ε_{min} being the liquid depth ratio of the TLD with the lowest being the liquid depth ratio.

2.2.8: Base shear force

As pointed out by Sun (1991), Fujino et al. (1992), Novo et al. (2014) and others, when a TLD is connected to a structure, there is a shear force generated in the opposite direction of the movement of the structure. This force is caused by the hydrostatic pressure of the liquid against the walls of the TLD and is known as the base shear force.

These authors propose that this base shear force creates an auto-equilibrated system with the excitation when the sloshing reaches its steady state, being the main cause of the energy dissipation mentioned before.

“The liquid-induced horizontal force acting on the walls of the tank is computed from hydrostatic pressure. The base shear force of the tank is the difference between the hydrostatic pressure in both sides of the walls. Contribution of forces due to frictions of side wall and bottom to the base shear force is small and neglected.” [Fujino et al., 1992]

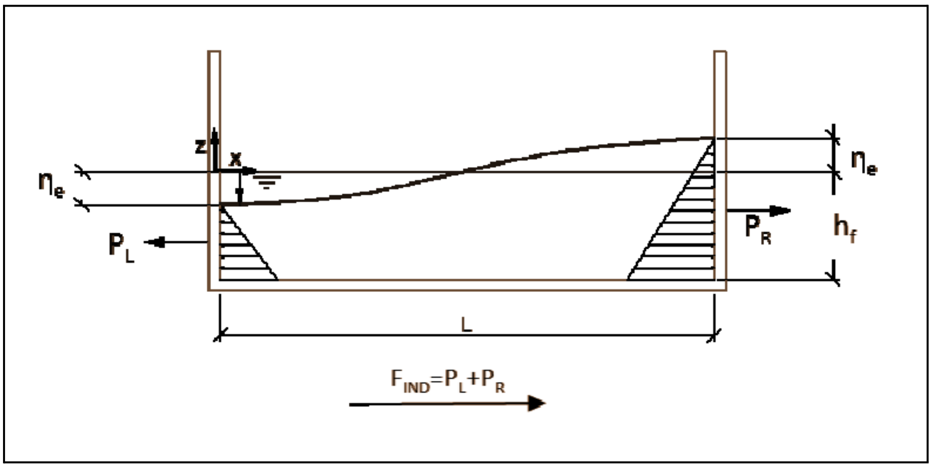

Figure 2.7 - Schematic representation of the forces induced to the structure due to fluid sloshing in a TLD. [Novo et al., 2012]

The shear force induced by fluid sloshing in a given instant can be determined through Equation 23.

$$F = \frac{\gamma \times b}{2} \times (h_{max}^{2} - h_{min}^{2}) \quad (23)$$

with: F being the base shear force the TLD applies on the structure [kN]; γ being the specific weight of the liquid [kN/m³]; b being the width of the TLD [m]; h_{max} being the maximum height the liquid inside the TLD reaches in a cycle [m]; and h_{min} being the minimum height the liquid inside the TLD reaches in a cycle [m].

2.2.9: Dissipation of energy

As is well known, being supported by many authors, including Clough (1975), the energy dissipated by the system in each cycle can be equated to the damping energy produced by it in that same cycle. This can be represented as a cycle of dissipation.

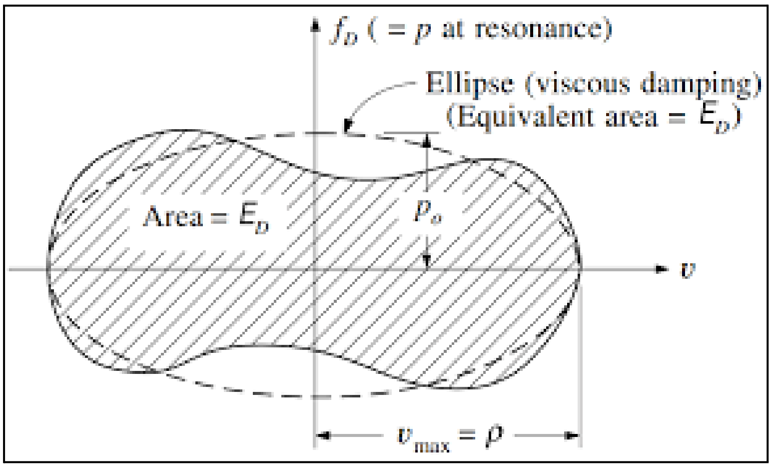

Figure 2.8 - Actual and equivalent damping energy cycle. [Clough, 1975]

In the case of TLD, as presented by Sun (1991), the shaking table inputs energy into the system and the TLD dissipates this energy due to the liquid sloshing. When the TLD has reached the steady state the energy inputted in the system will equal the energy dissipated by the TLD. This energy can be determined through a cycle of dissipation (Equation 24).

$$\Delta E = \int_{1}^{1+T} F(t) \times u(t) \times dt \tag{24}$$

with: ΔE being the energy dissipated by each cycle [MJ]; T being the period of excitation [s]; $F(t)$ being the base shear force the TLD applies on the structure in an instant t [kN]; $u(t)$ being the total displacement of the TLD in an instant t [m]; and t being the time (s).

The cycle of dissipation can also be used to calculate the damping coefficient of a system in its resonance frequency as noted by Clough (1975) and Novo et al. (2014).

"If the structure has linear viscous damping, the curve will be an ellipse [...]. In this case, the damping coefficient can be determined directly from the ratio of the maximum damping force to the maximum velocity, where it is noted that the maximum velocity is given by the product of frequency and displacement amplitude. If the damping is not linear viscous, the shape will not be elliptical [...]. In this case, an equivalent viscous damping coefficient can be defined which would cause the same energy loss per circle [...]. In other words, the equivalent viscous damper is associated with the elliptical force-displacement diagram having the same area and maximum displacements as the actual force diagram" [Clough, 1975]

This ratio can be simplified and when divided by the critical damping resulting in the damping coefficient.

$$\xi = \frac{\Delta E}{2 \times \pi \times k \times u_{max}^{2}} \tag{25}$$

with: ξ being the damping coefficient; ΔE being the energy dissipated by each cycle [MJ]; k being the stiffness of the structure [MN/m]; and u_{max} being the maximum displacement of the structure [m].

3

METHODOLOGY

3.1: Introduction

The TLD in study, as mentioned before, was designed to be used to control the vibration of industrial chimneys. The chimneys in question were tested by the partner company and its characteristics were shared for a better simulation of their behaviour.

The chimneys' height is 65 m and their external diameter is 3.08 m. The frequency of their first mode of vibration ranged from 0.65 Hz to 0.78 Hz depending on the integrity of the structure (the more corroded the chimney, the higher its natural frequency), their damping coefficient is small, lower than 1%, and the stack displacements without damping reached 0.5 m.

According to NP EN 1991-1-4 proposed method, the amplitude of vibration in the first mode should not exceed the indicative value of acceptable vibrations of 5% the external diameter of the chimney when making an assessment of the vortex-shedding amplitude of vibration of the stack. For the ones in question in this study, the desired displacement amplitude is, therefore, 15 cm or less.

As the laboratorial tests were envisioned to be carried out with the use of a shaking table, it was decided that a pendulum could be used as a model for the original structure due to their low damping coefficient and high displacement (even for small excitation).

3.2: Experimental apparatus and procedure

3.2.1: Shaking table

The shaking table used in this study was made with Tecnogial's and Equinotec's technology. It has a surface area of 3x3 m^2 and has a maximum amplitude of 440 mm in both main axes (xx and yy - both horizontal) and also has movement capability on its third axis (zz - vertical). The table can reach frequencies of up to 30 Hz and a maximum speed of 67 mm/s with a maximum load of around 10 tons.

Despite the massive capabilities of the shaking table, it is well adjusted to perform tests with very low amplitudes and frequencies as well, as is the case in this study. For the study in question only one of the main axes will be in use and its amplitude was reduced to a maximum of 5 mm.

3.2.2: Small scale model

A structure made out of wooden rafters with a 35×55 mm² cross section was constructed to serve as the support of the pendulum made out of cables connected to a wooden box designed to hold the TLD reservoir and additional masses.

The wooden structure was fixed to the shaking table with 18 mm thick wooden plates of 200x200 mm² surface that were tightened with screws and clamps. The pendulum's box was made out of the same plates and rafters as the rest of the woodwork with an usable area of 785×630 mm².

The pendulum's length was defined as 505 mm due to the height of the reservoir and the thickness of the steel plates used as the additional mass (dimensions specified below). The cables that create the pendulum were braced so as to impose a single axis of movement. With the specified length, through Equation 8, the oscillatory frequency was calculated.

$$f_w = \frac{1}{2\times\pi} \times \sqrt{\frac{9.81}{0.505}} = 0.698\,Hz$$

With the pendulum oscillatory frequency within the range of the chimneys' for which the TLD might be implemented natural frequencies, it was deemed as an adequate analogue to them.

The mass to be considered for the structure has two components, the mass of the pendulum, which was about 9.5 kg, and an additional mass comprised of four 600×300×20 mm³ steel plates, each of which weighing approximately 28.08 kg ($m_{str} = 0.6 \times 0.3 \times 0.02 \times 7800 = 28.08$ kg), and an undetermined number of 600x150x10 mm³ steel plates, each of which weighing approximately 7.15 kg. The number of the latter steel plates in use will depend on the height of water in the reservoir and will be defined in the Section 3.2.4.

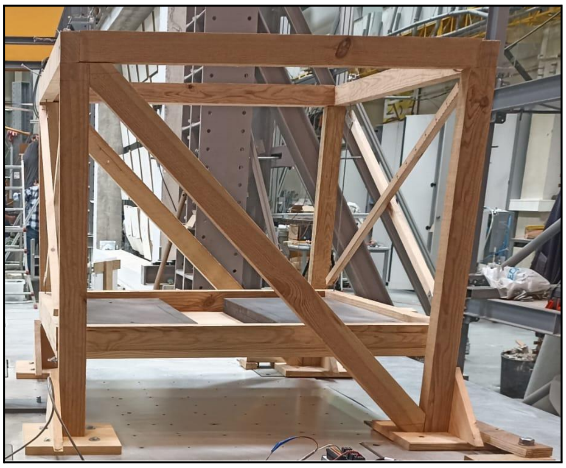

Figure 3.1 - Small scale model fixed to the shaking table.

3.2.3: Big scale model

The big scale model was also a pendulum with length defined as 505 mm to match the oscillatory frequency of the small scale model. Built with four hollow metallic columns supporting two hollow metallic beams with a cross section of 9×9 cm², 5 mm thick and with a length of 1.7 m, weighing approximately 12 kg in total. Three steel rebars with diameter of 30 mm and length of 3 m, weighing approximately 50 kg in total were used to connect the hollow beams.

The wooden structure was made of eight 7.5×7.5 cm² cross section rafters of different lengths, weighing approximately 35 kg in total. In addition to the wooden structure, a concrete slab of approximate surface area of 2×2 m² and thickness of 8.5 cm is used as mass, weighing about 816 kg was also added to the structure.

Figure 3.2 - Big scale model with the quarter-ring TLD fixed to the shaking table.

3.2.4: Rectangular reservoir

The rectangular reservoir used on the initial tests was made out of 1 mm thick transparent acrylic plates with its internal dimension of 600×400×400 mm³.

Figure 3.3 - Rectangular reservoir.

The height of water to be used was defined with Equation 9 equating the sloshing frequency with the frequency of the structure.

$$0.698 = \frac{1}{2\times\pi} \times \sqrt{\frac{\pi\times 9.81}{0.6} \times tanh(\frac{\pi\times h_f}{0.6})} \Leftrightarrow h_f = 0.075\, m$$

With this height of water, the mass of the water inside of the TLD is approximately 18 kg ($V_f = 6 \times 4 \times 0.75$ = 18 dcm³) and the acrylic reservoir itself weighs about 12.25 kg and will be included in the mass of the structure as it does not have damping capabilities.

With these informations, the ratio of masses can be determined as per Equation 16.

$$\mu = \frac{18}{(4\times 28.08)+12.25+9.50+(n\times 7.15)}$$

with: n being the number of steel plates.

The solution adopted utilised six steel plates, resulting in $\mu = 10.17\%$ which was considered adequate for the purposes of this study.

The liquid depth ratio can be determined as per Equation 17.

$$\varepsilon = \frac{7.5}{60/2} = 0.25$$

This is not ideal, but as the ratio is not far from 0.2, it was decided that this should be enough to create an effective damper.

3.2.5: Annular reservoir

The annular reservoir to be used as the basis for this study was developed by Modalyse Engineering, it was designed to be built with steel sheets and has an external diameter of 3932 mm and an internal diameter of 3080 mm. Its height is 492 mm and the divisions are made with thin steel sheets creating 20 cells of equal dimensions, the divisions have a height of 458 mm and two triangular punctures in their base allowing the liquid to travel between the cells. This means that each cell comprises a slice that makes an angle of 18º to the centre of the ring and would be similar in shape to a rectangle of sides 551×426 mm².

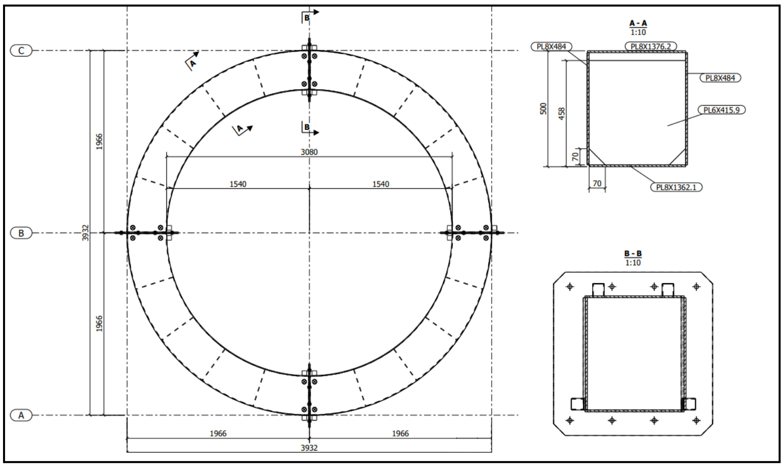

Figure 3.4 - Schematics of the annular TLD. [Modalyse]

A reservoir with the dimensions of one of the cells of the annular reservoir was built in order to perform a second battery of tests with the small scale model. This reservoir bottom and rectilinear walls were made out of 15 mm thick plywood rigid panels and the curved walls out of 4 mm thick plywood flexible panels. The interior joints of the reservoir were closed with white silicone rubber to prevent leaking and all the interior surface was covered by a layer of white liquid silicone rubber to coat the plywood with an impermeable protection.

The dimensions of the base constitute a 1/20 portion of a ring whose internal diameter is 3080 mm and external diameter is 3932 mm. Each rectilinear wall has a length of 426 mm and an internal height of 280 mm. The curved walls have a length of approximately 618 mm (external) and 484 mm (internal) and both have an internal height of 280 mm.

Figure 3.5 - Reservoir built like a cell of the annular reservoir.

Assuming the hypothesis that the cell of the reservoir will behave like a rectangular one of similar size (551×426 mm²), the height of water can be defined with Equation 9, similarly to what was done with the rectangular TLD. In this case, the length used was 426 mm because in a ring configuration this is how the main acting cell will be aligned to the excitation.

$$0.698 = \frac{1}{2\times\pi} \times \sqrt{\frac{\pi\times 9.81}{0.426} \times tanh(\frac{\pi\times h_f}{0.426})} \Leftrightarrow h_f = 0.037\, m$$

With this height of water, the mass of the liquid inside of the TLD is approximately 8.68 kg ($V_f = 5.51 \times 4.26 \times 0.37 = 8.68$ dcm³). As the reservoir itself weighs only about 7.22 kg it was decided to increase the number of steel plates utilised on the previous tests by one to keep the weight of the structure closer to the previous iteration. The ratio of masses can be determined as per Equation 16 And with the set height of water, it is also possible to determine the liquid depth ratio with Equation 17.

$$\mu = \frac{8.68}{(4\times 28.08)+7.22+9.50+(7\times 7.15)} = 4.85\% \qquad \varepsilon = \frac{3.7}{42.6/2} = 0.17$$

These parameters were deemed adequate for the purposes of this study and are comparable to what was used on the second iteration of tests performed with the rectangular TLD (see Section 4.2 of this study).

For the tests with the big scale model, due to the dimensions of the designed TLD, it was decided that only a quarter-ring TLD built following the same design (external radius of 1966 mm, internal radius of 1540 mm and divisory plates every 18º) and built with 2 mm thick welded steel sheets would be used for the tests, this reservoir weights about 78 kg. As the effect of a TLD is cumulative, this will not introduce errors to the results, although the damping provided will be greatly diminished (to about 30-40% of the expected damping provided by the full TLD).

Figure 3.6 - Quarter-ring reservoir.

3.2.6: Sensors

For the small scale model, measurements were taken using two sensors: a liquid level sensor and a proximity sensor. The first one was a Milone Technologies' 12 inches (30 cm) eTape™ and the latter, a sensor from the GP2Y0A51SK0F line from the Sharp Corporation with a range of 2-15 cm. The water level sensor measures the hydrostatic pressure of the fluid through a variation in its internal resistance (which gets lower when the liquid level rises) and the proximity sensor outputs a voltage corresponding to the detection distance (which lowers when the distance increases).

Both sensors were manually calibrated using a linear regression for the water level sensor and a polinomial regression for the proximity one. In both cases, the calibration results were a close match to the manufacturer's specifications. The calibration curve of each sensor can be seen in Figures 3.7 and 3.8.

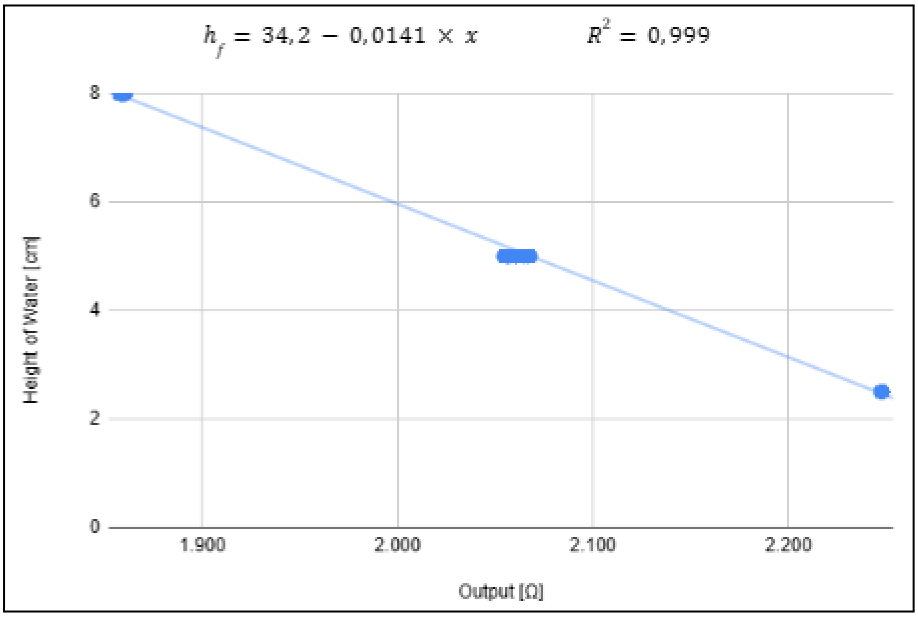

Figure 3.7 - Water level sensor's calibration curve

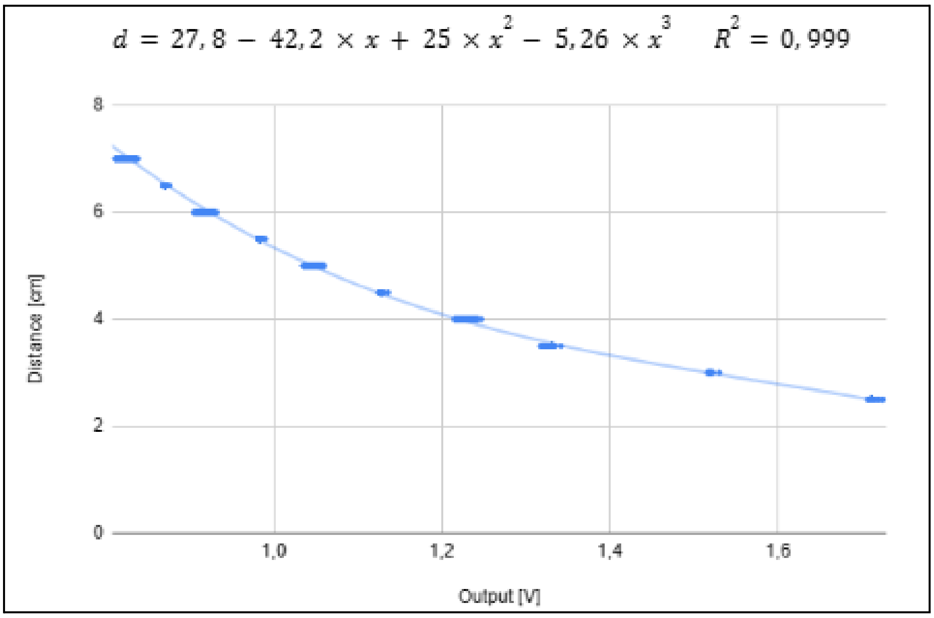

Figure 3.8 - Proximity sensor's calibration curve

The eTape was submerged in the liquid and fixed to the wall of the TLD with a 3D printed support and the Sharp sensor was fixed to the shaking table with a 3D printed support, both supports were designed, printed and assembled “in house”.

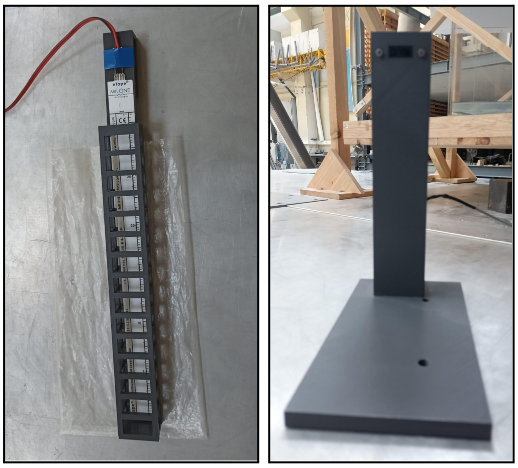

Figure 3.9 - Water level sensor (left) and proximity sensor (right) in their final form.

For the big scale model, an accelerometer was used due to physical constraints while using the previously mentioned Sharp sensor. The acquisition frequency was 62.5 Hz and output was the measurement in all axes, although only the excited axis (zz with the device as the reference point) was analysed. The data was collected in counts per second and then converted to acceleration through Equation 26 and finally to displacement through Equation 27.

$$u''(t) = z(t) \times \frac{1}{20^{20}} \times 4 \times 9.81 \tag{26}$$

with: $u''(t)$ being the acceleration [m/s²]; and $z(t)$ being the sensor’s output [counts/s]

$$u(t) = \frac{u''(t)}{\omega^2} \tag{27}$$

with: $u(t)$ being the displacement [m]; $u''(t)$ being the acceleration [m/s²]; and ω being the natural frequency of the structure [rad/s]

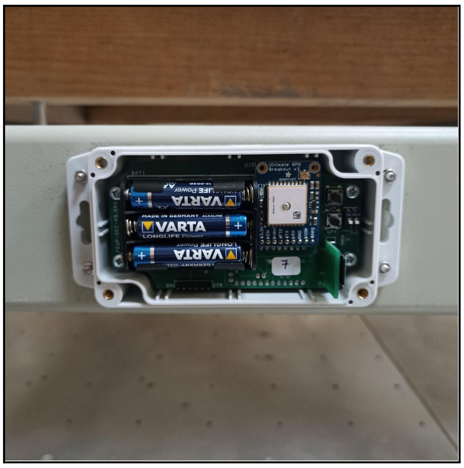

Figure 3.10 - Accelerometer.

3.2.7: Data acquisition and processing system

The data acquisition was done through a National Instruments' NI-9219 and NI-9215 universal analog input modules connected to a NI cDAQ-9178 compactDAQ chassis integrated with National Instruments' LabVIEW software.

LabVIEW was chosen as the processing system because of its intuitive nature and to keep all of the code related to the study in the same language (in this case a "graphical programing language"), as the shaking table controls were already developed in that software.

The data processing system was created in LabVIEW using the program DAQ Assistant function. The water level sensor used a continuous sampling with a rate of 100 Hz and a signal input range of 1500 to 2500 Ω. The proximity sensor used a continuous sampling with a rate of 10000 Hz and a signal input range of 0 to 3 V. Due to noisy signals from the proximity sensor, it received further processing through a lowpass type filter with a cutoff frequency of 20Hz and a realignment and resampling process with the resampling interval of 0.01; both of these procedures were performed with LabVIEW standard functions.

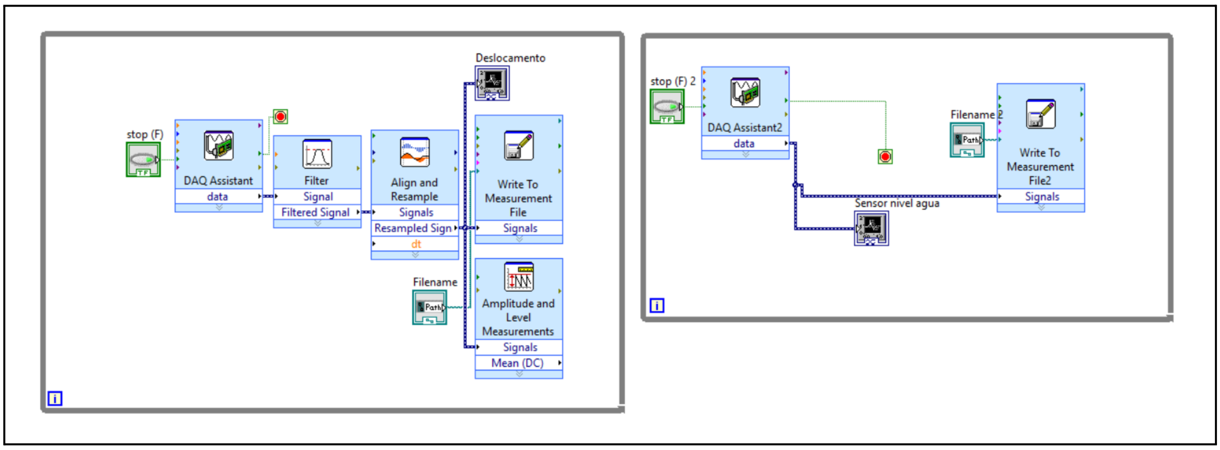

Figure 3.11 - LabVIEW code.

Once the data from the sensors was collected, it was transferred to a Google Sheets document for further processing, namely converting the results from the sensor's output to the variables of interest through the calibration curves already mentioned, the plotting of the results (to quickly narrow down the data collected to a useful interval) and evaluating the steady state response and the decay of displacement in free vibration of the data.

A Fourier's transformation using an FFT algorithm was performed with MathWorks' MATLAB software in order to guarantee that the imputed frequency was the desired one. The result of this analysis was that the principal excitation was acting on the desired frequency, however there was also some interference at the higher multiples of the desired frequencies. This is not expected to have a great impact and was also noticed by prior researchers, such as Welt (1988).

4

RESULTS AND DISCUSSION

4.1: Tests with the rectangular reservoir

The initial tests were performed with the rectangular reservoir set directly on the shaking table with the goal of evaluating the applicability of the formulas for sloshing frequency and damping of liquid motion in the current study and also to determine how the water would behave when the reservoir was subjected to an excitation that was not parallel to one of its main axes (when the reservoir was rotated on the shaking table).

Table 4.1.1 contains the conditions in which each test was performed as well as the expected results in the cases where there are equations to predict the behaviour of the liquid.

Table 4.1.1 - Information about the tests with the rectangular reservoir

Test ID	Excitation angle to the longer side of the TLD	Height of water [cm]	Base displacement amplitude [mm]	Expected sloshing frequency [Hz]
$01\alpha0$	0º	8	0.50	0.72
$01\alpha30$	30º	8	0.50	-
$01\alpha45$	45º	8	0.50	-
$01\alpha60$	60º	8	0.50	-
$01\alpha90$	90º	8	0.50	1.04

For all configurations, there was performed a sweep frequency test in a predetermined frequency range through the utilisation of discrete points (0.02 Hz apart or 0.01 Hz apart while near the resonant frequency) each of which was excited for 10 minutes in order to determine the steady state response of the liquid.

The conventional sweep frequency test was neglected in this study due to interferences caused by beatings that would not give an accurate reading of the liquid response as the response for a frequency leaks into the response of the following frequencies.

For $01\alpha0$ and $01\alpha90$ the tests were performed with a frequency range close to the expected one (0.70 to 0.80 Hz for $01\alpha0$ and 1.00 to 1.10 Hz for $01\alpha90$). For the other cases, the tests were made in both of these ranges with the intention to cover the intermediary frequencies (0.80 to 0.90 Hz) if necessary.

The measurements of the variation of the liquid level were recorded for all the tested frequencies in all the different configurations both while the excitation was present and also in free vibration until this displacement reached an insignificant value.

The steady state response of the liquid in the different frequencies for each configuration was then plotted, creating the frequency-response graphs presented in Figures 4.1.1, 4.1.2, 4.1.3, 4.1.4 and 4.1.5, in order for the resonating frequency of the liquid to become evident in each case.

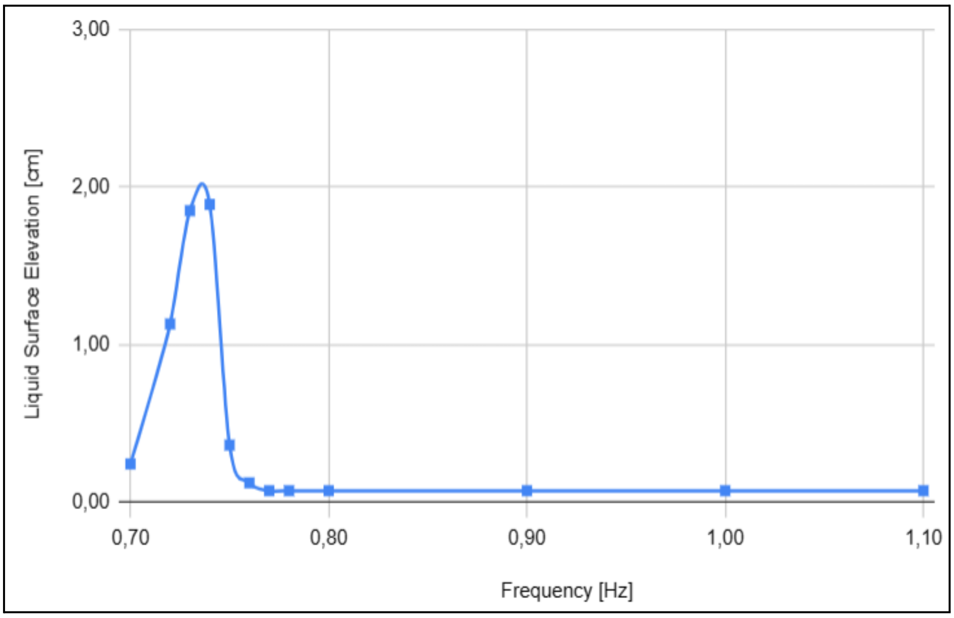

Figure 4.1.1 - Frequency-response in the steady state in configuration 01α0

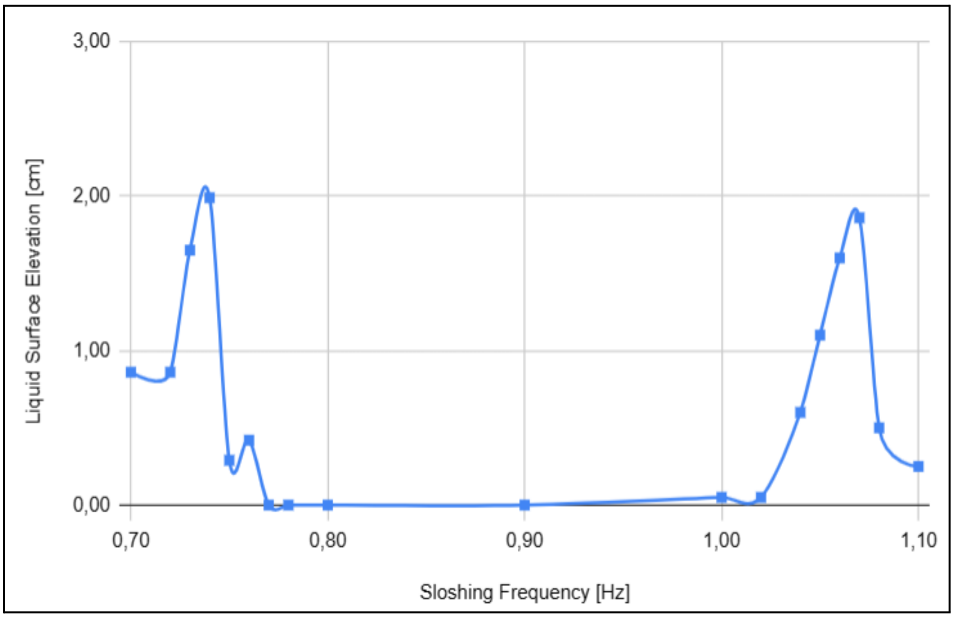

Figure 4.1.2 - Frequency-response in the steady state in configuration $01\alpha30$

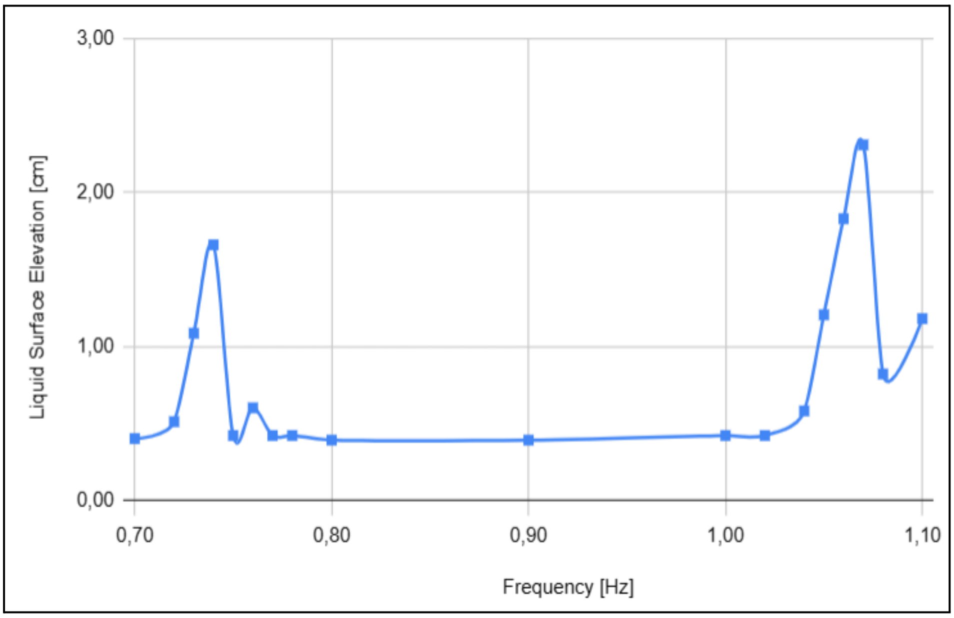

Figure 4.1.3 - Frequency-response in the steady state in configuration $01\alpha45$

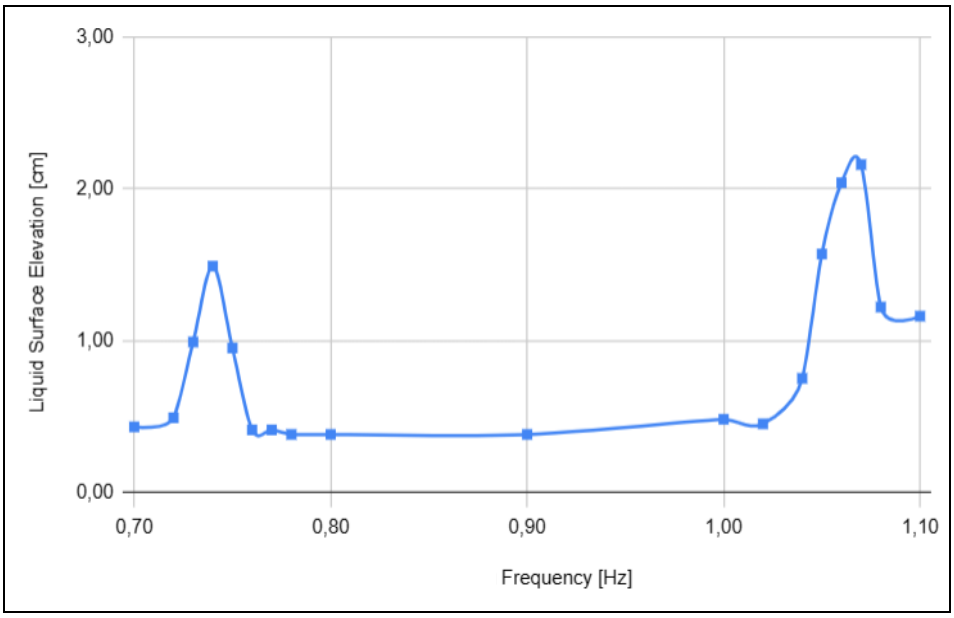

Figure 4.1.4 - Frequency-response in the steady state in configuration $01\alpha60$

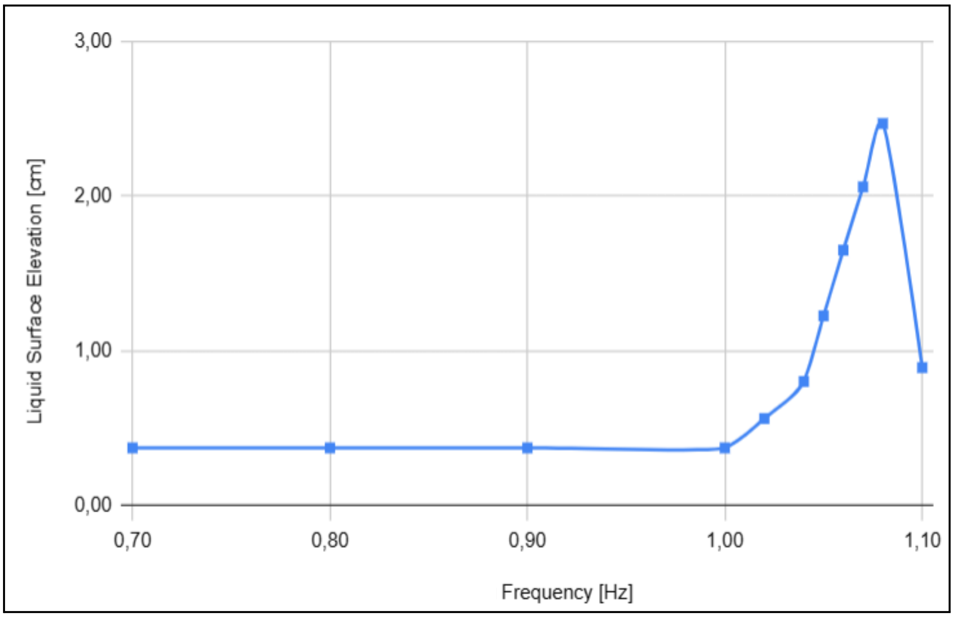

Figure 4.1.5 - Frequency-response in the steady state in configuration $01\alpha90$

The behaviour of the reservoir in its main axes was close to what was expected, the maximum surface elevation in steady state occurring when the frequency was 0.74 Hz for $01\alpha0$ and 1.08 Hz for $01\alpha90$ (an increase of 2.8% and 3.8% respectively when compared to the analytical value).

For $01\alpha30$, $01\alpha45$ and $01\alpha60$ it was observed that, no matter the angle the excitation made with the main axes of the reservoir, the liquid behaved as if it was being excited in those main axis according to the frequency of excitation, i.e. when the frequency was close to 0.74 Hz, the liquid behaved similarly to its behaviour in 01α0 and, when the frequency was close to 1.08 Hz, to its behaviour in 01α90, as is schematized in Figure 4.1.6. This resulted in two frequencies appearing as a resonance behaviour.

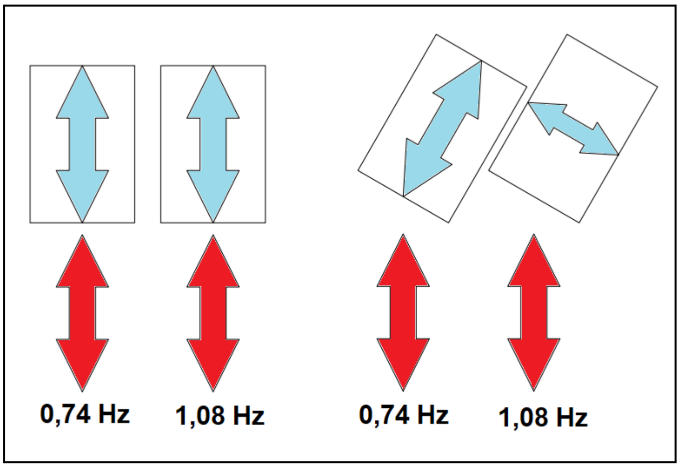

Figure 4.1.6 - Example of the behaviour of the liquid in the reservoir (blue) based on the excitation (red) in different frequency ranges.

The damping of liquid motion for the resonant frequency (or frequencies in configurations 01α30, 01α45 and 01α60) was calculated using Equation 12 with the liquid surface elevation measured in the steady state phase of the response. For 01α30, 01α45 and 01α60 the width utilised in the equation was assumed based on the behaviour of the water, because of the aforementioned similarity of the liquid behaviour and the movement of the water in their main axes.

A summary of the information gathered in these tests is presented in Tables 4.1.2 and 4.1.3.

Table 4.1.2 - Results of tests with the rectangular reservoir with excitation frequency near 0.74 Hz

Test ID	Liquid surface elevation [cm]	Sloshing frequency [Hz]	Damping of liquid motion [rad/s]
01α0	1.78	0.74	0.0148
01α30	1.88	0.74	0.0146
01α451	1.55	0.74	0.0151
01α60	1.38	0.74	0.0154

Table 4.1.3 - Results of tests with the rectangular reservoir with excitation frequency near 1.08 Hz

Test ID	Liquid surface elevation [cm]	Sloshing frequency [Hz]	Damping of liquid motion [rad/s]
$01\alpha30$	1.75	1.07	0.0168
$01\alpha45$	2.20	1.07	0.0161
$01\alpha60$	2.05	1.08	0.0163
$01\alpha90$	2.36	1.08	0.0159

As can be seen, the configuration $01\alpha30$ had a symmetrical behaviour between its lower resonance response and its higher one, but, with the increasing of the rotation in configurations $01\alpha45$ and $01\alpha60$, the response in the higher resonance became more prevalent.

The damping of liquid motion was low in general, despite the high surface elevation reached, as was expected due to water being the liquid in study.

4.2: Interaction of the rectangular TLD with the small scale structure

This section will deal with the tests with the rectangular reservoir mounted on the small scale structure, therefore acting as a TLD. Initially tests with just the pendulum were performed to confirm its natural frequency. Figure 4.2.1 contains the frequency-response curve of these tests.

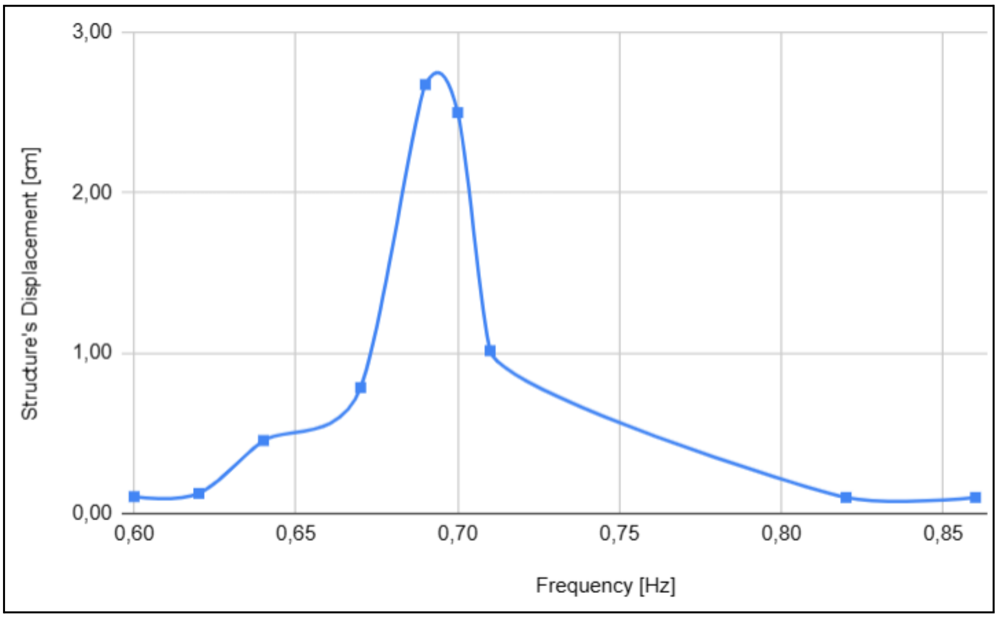

Figure 4.2.1 - Frequency-response of the smaller pendulum in the steady state.

As can be seen in the curve, the resonant frequency was 0.69 Hz, which is very close to what was previously calculated. The damping coefficient of the structure was determined through the decay of free vibrations. This was carried out through the plotting of the results in a graph and with an exponential regression as displayed in Figure 4.2.2 and then with the application of equation 7.

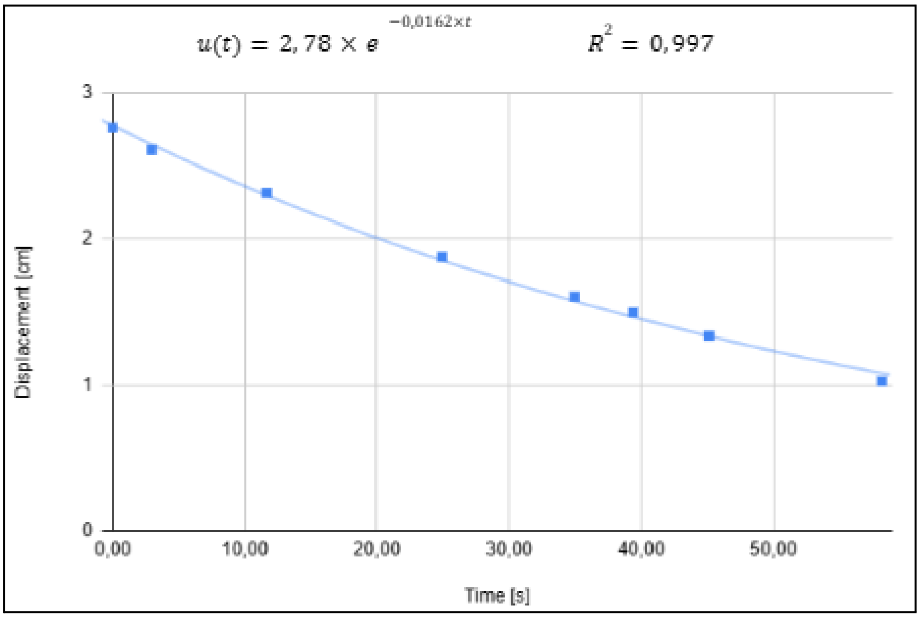

Figure 4.2.2 - Decay of free vibration of the smaller pendulum starting at its steady state response.

$$u(t) = 2.78 \times e^{-0.0162\times t} \Leftrightarrow$$

$$\Leftrightarrow e^{-\xi\times\omega\times t} \times [u_o \times cos(\omega_d \times t) + \frac{u'_o + u_o \times \xi \times \omega}{\omega_d} \times sen(\omega_d \times t)] = 2.78 \times e^{-0.0162\times t} \Leftrightarrow$$

$$\Leftrightarrow -\xi \times \omega \times t = -0.0162 \times t \Leftrightarrow \xi = 0.37\%$$

Table 4.2.1 - Results of tests with the smaller pendulum

Oscillation frequency [Hz]	Structure's displacement [cm]	Structure's damping coefficient
0.69	2.68	0.37%

The displacement of the pendulum is significant (although still inside of the allowed by the maximum established amplitude of 15 cm) and its damping coefficient, as expected, was very small, being nearly negligible.

When combining the structure with the TLD, there will be a two masses system at work. As previously mentioned, if the TLD is well tuned to the structure, it will result in a two peaked frequency-response curve with its lowest point near the frequency of the structure. Table 4.2.2 contains the conditions in which each test was performed.

Table 4.2.2 - Information about the tests with the rectangular TLD and the small scale structure

Test ID	Excitation angle to the longer side of the TLD	Height of water [cm]	Base displacement amplitude [mm]
02α0	0º	7.5	0.50
02α5	5º	7.5	0.50
02α10	10º	7.5	0.50
02α15	15º	7.5	0.50
02α30	30º	7.5	0.50
02α45	45º	7.5	0.50
02α60	60º	7.5	0.50

Similarly to what was previously done, a sweep frequency test utilising discrete points (0.02 Hz apart or 0.01 Hz apart while near a resonant frequency) each of which was excited for 10 minutes in order to determine the steady state response of the structure starting in 0.69 Hz and going in both directions was performed for the 02α0 configuration to discover what were the new resonant frequencies.

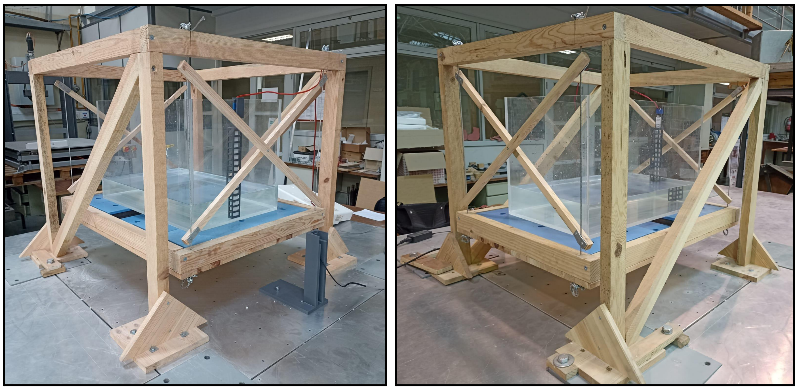

Figure 4.2.3 - Small scale structure with the rectangular reservoir in configuration 02α0.

As can be seen in Figure 4.2.4, the lower resonant frequency was 0.62 Hz and the higher one was at 0.82 Hz. It is important to point out that for the frequencies nearer to the lower resonant frequency there was a noise that was not expected nor perceived in the previously performed reservoir tests.

In these frequencies (0.60 to 0.67), it was clear that two waves were being formed on the liquid and, specifically in the 0.62 Hz, the noise reached a point in which the waves were close to the breaking point and a wave in the other main axis was also in effect.

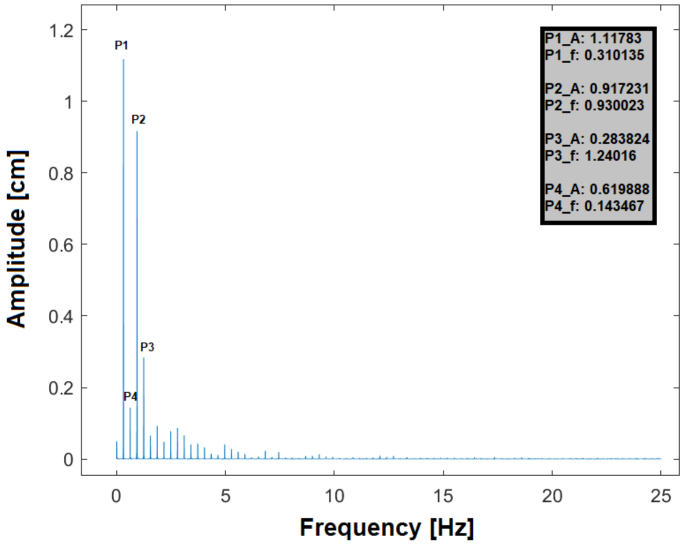

Figure 4.2.4 - Results of the FFT for liquid surface elevation measurements in configuration 02α0 at frequency 0.62 Hz.

As neither of the previously mentioned effects appear to have any major impact on the behaviour of the pendulum, which kept a sinusoidal movement throughout and the FFT algorithm did not point out the acting of a frequency other than the multiples of 0.62 Hz, it was decided that this should not invalidate the measurements of the structure’s response.

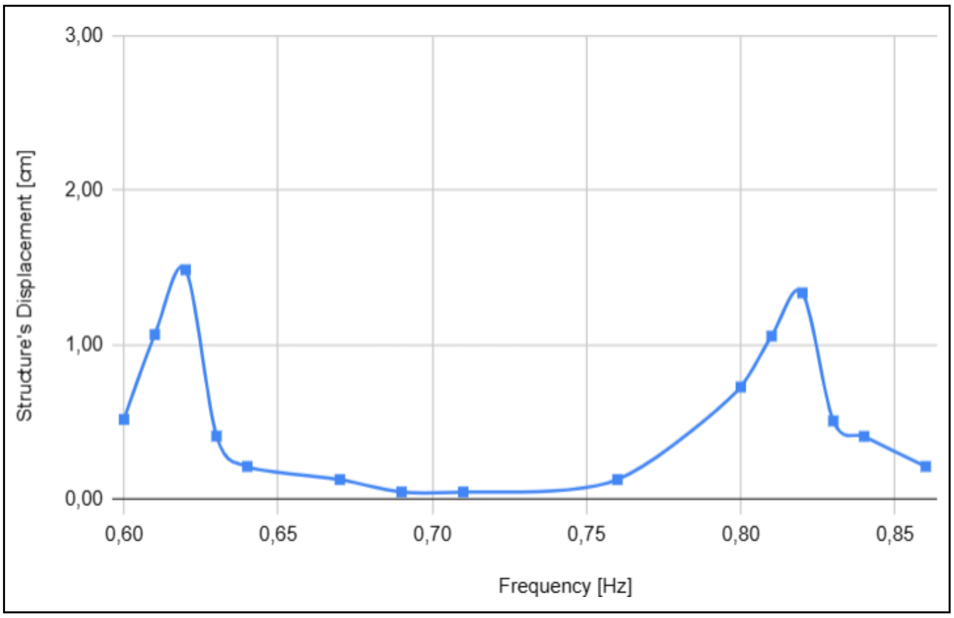

Figure 4.2.5 - Frequency-response of the system in the steady state in configuration $02\alpha0$.

Due to the response observed in the rotated reservoirs in the previous tests, it was decided that for the other configurations the frequency range in which the tests were performed should be the same as the one used for $02\alpha0$, as their lower sloshing frequency should be the same as, or at least very close to, the latter's one.

The excitation frequencies utilised in these tests were: 0.60 Hz, 0.61 Hz, 0.62 Hz, 0.63 Hz, 0.64 Hz, 0.67 Hz, 0.69 Hz, 0.71 Hz, 0.76 Hz, 0.80 Hz, 0.82 Hz, 0.83 Hz, 0.84 Hz and 0.86 Hz. These points were chosen to optimise the tests as the responses in these frequencies are enough to create a good aligned frequency-response curve that spans both of the resonant frequencies with most of the omitted frequencies not being relevant to the present study. Although, for the higher rotations (configurations $02\alpha30$, $02\alpha45$ and $02\alpha60$) more points were required due to a higher variation of the resonant frequency in these cases.

It is expected that there would be some interaction between the liquid sloshing at its higher sloshing frequency (i.e. in the sloshing frequency reached when the reservoir is rotated 90º) in these configurations and the structure, however, in a real situation, it would be rare for that to be relevant and it would be out of the scope of this study, therefore, it is not be justifiable to further investigate this interaction.

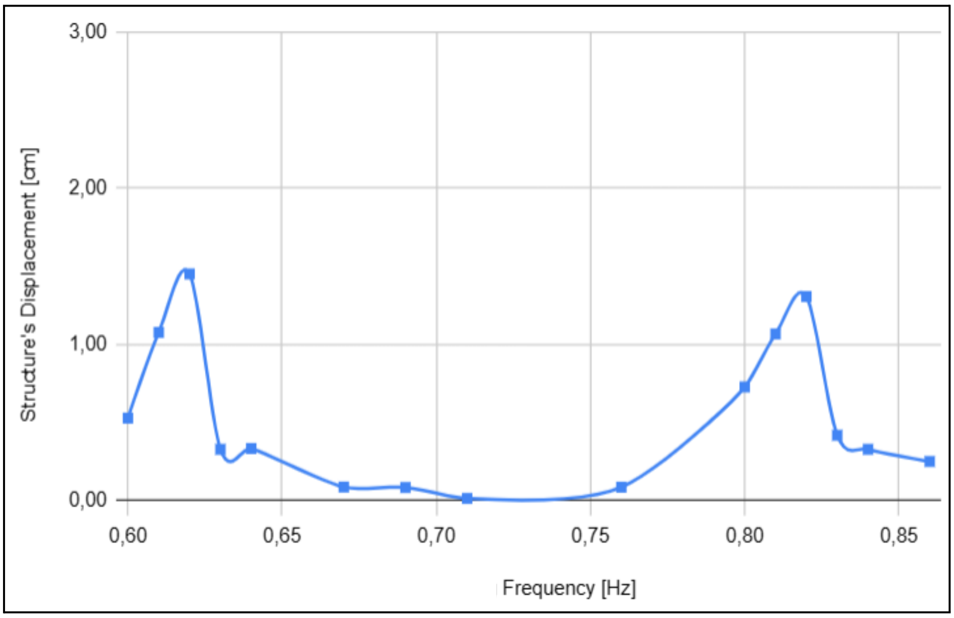

Figure 4.2.6 - Frequency-response of the system in the steady state in configuration $02\alpha5$.

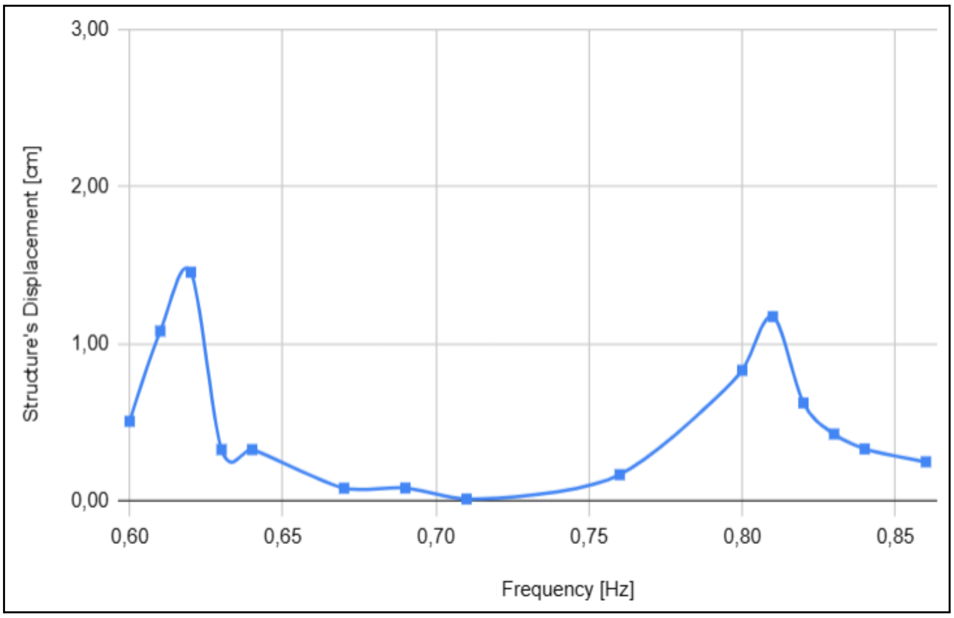

Figure 4.2.7 - Frequency-response of the system in the steady state in configuration $02\alpha10$.

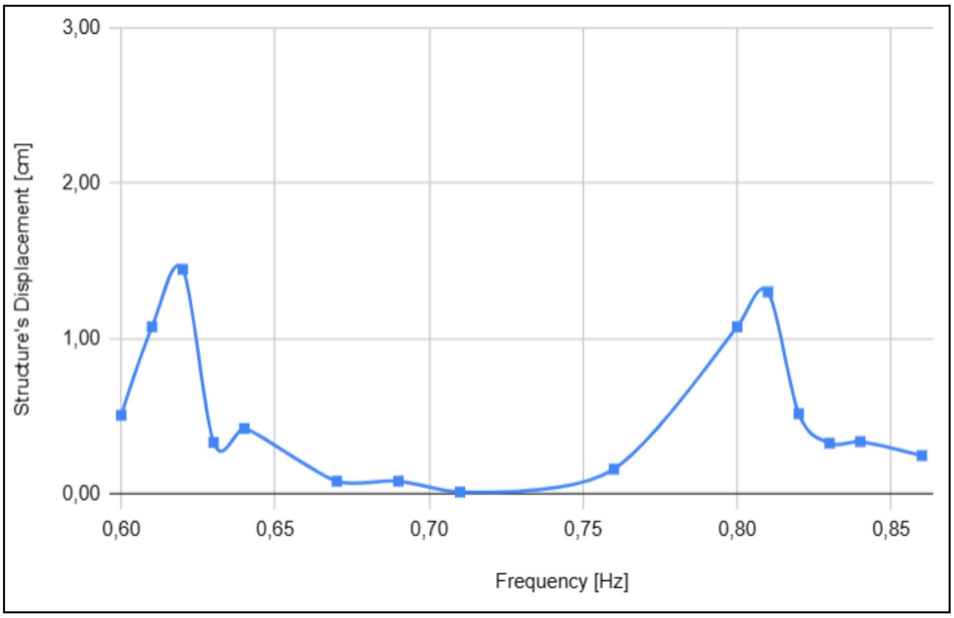

Figure 4.2.8 - Frequency-response of the system in the steady state in configuration $02\alpha15$.

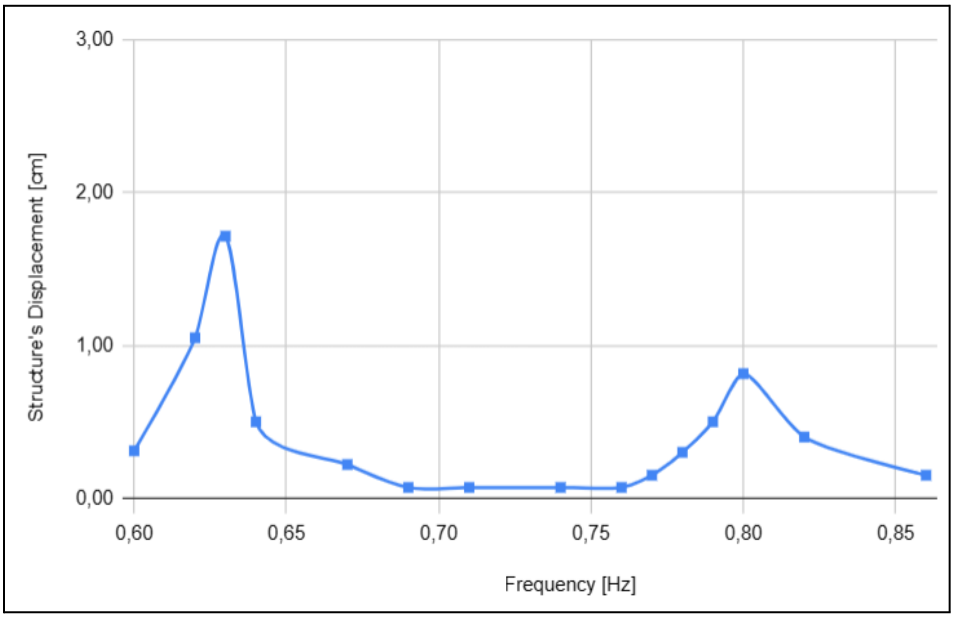

Figure 4.2.9 - Frequency-response of the system in the steady state in configuration $02\alpha30$.

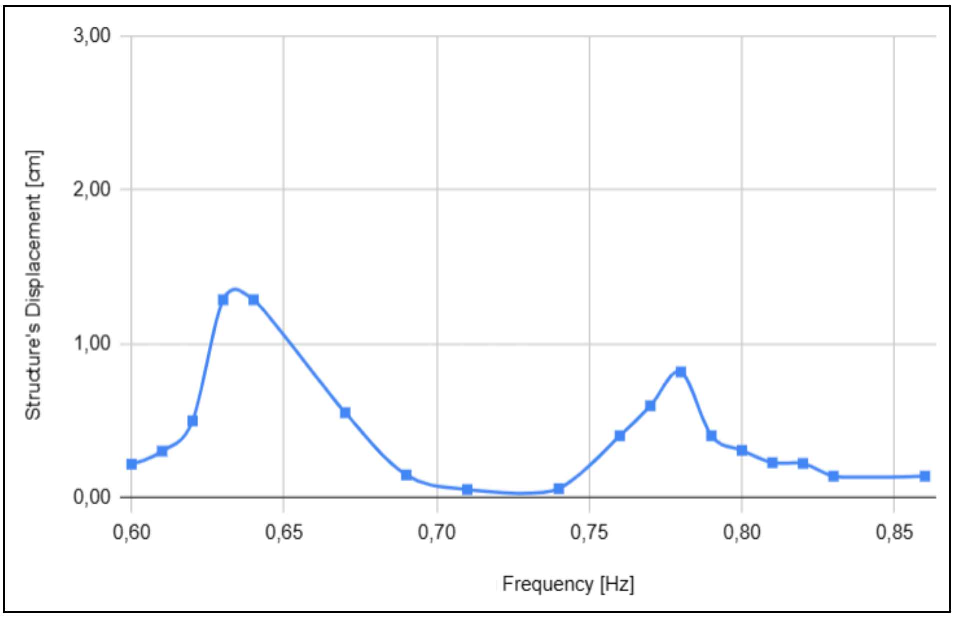

Figure 4.2.10 - Frequency-response of the system in the steady state in configuration $02\alpha45$.

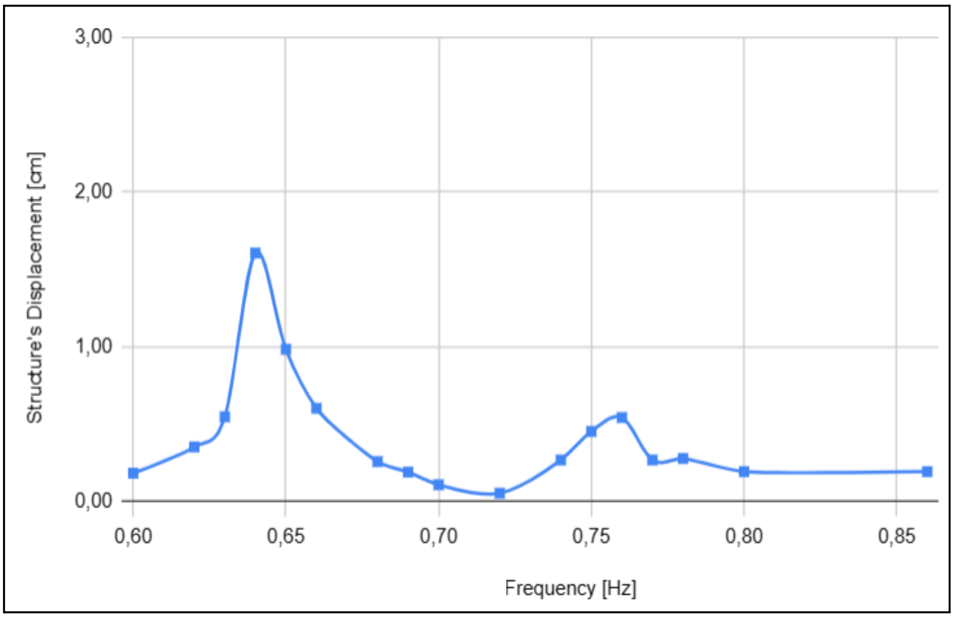

Figure 4.2.11 - Frequency-response of the system in the steady state in configuration $02\alpha60$.

Table 4.2.3 - Results of tests with the rectangular TLD for the multiple configurations with the excitation frequency at their lower resonant frequency

Test ID	Resonant frequency [Hz]	Liquid surface elevation [cm]	Damping of liquid motion [rad/s]	Expected damping increase	Structure's displacement [cm]	System's damping coefficient
$02\alpha0$	0.62	2.91	0.0321	0.41%	1.49	0.48%
$02\alpha5$	0.62	3.00	0.0318	0.41%	1.45	0.45%
$02\alpha10$	0.62	2.90	0.0321	0.41%	1.46	0.51%
$02\alpha15$	0.62	3.06	0.0317	0.41%	1.45	0.49%
$02\alpha30$	0.63	2.99	0.0321	0.41%	1.72	0.45%
$02\alpha45$	0.64	2.43	0.0342	0.43%	1.29	0.34%
$02\alpha60$	0.64	2.28	0.0348	0.43%	1.61	0.42%

Table 4.2.4 - Results of tests with the rectangular TLD for the multiple configurations with the excitation frequency at their higher resonant frequency

Test ID	Resonant frequency [Hz]	Liquid surface elevation [cm]	Damping of liquid motion [rad/s]	Expected damping increase	Structure's displacement [cm]	System's damping coefficient
$02\alpha0$	0.82	2.87	0.0371	0.36%	1.34	0.43%
$02\alpha5$	0.82	2.80	0.0373	0.36%	1.31	0.44%
$02\alpha10$	0.81	2.37	0.0387	0.38%	1.17	0.44%
$02\alpha15$	0.81	2.65	0.0377	0.37%	1.30	0.42%
$02\alpha30$	0.80	2.24	0.0390	0.39%	0.82	0.37%
$02\alpha45$	0.78	2.80	0.0364	0.37%	0.82	0.50%
$02\alpha60$	0.76	2.50	0.0370	0.39%	0.54	0.31%

As can be seen in the results presented above, the structure's response when in resonance was reduced in all configurations for both their lower and higher resonance frequencies. This attenuation of nearly 50% (reaching upward to 80% in $\beta60$ higher resonance) would indicate that the damping should have doubled.

This increase in damping would be equivalent to the expected increase caused by the liquid sloshing, because, despite the surface elevation of the water reaching 2.24 cm at its lowest in $02\alpha30$

higher resonant frequency (a 30% increase from the initial water level), only a small absolute increase in the damping coefficient was expected based on the results obtained through Equation 12.

Configurations $02\alpha0$, $02\alpha5$, $02\alpha10$ and $02\alpha15$'s results were very similar to one another, which means that these lower rotations did not have a great impact on the tuning of the TLD. The lower resonant frequency appeared at 0.62 Hz for all configurations and there was but a small variation of the higher one's location on the frequency range.

In all cases, the response of the structure at both resonance states was reduced to around half. Reaching values in the range of 1.45 to 1.50 cm for the lower resonant frequency and in the range of 1.30 to 1.35 cm for the higher one, with the exception of $02\alpha10$'s results with the structure's maximum displacement only reaching 1.17 cm for the latter frequency.

There was an increase in the damping coefficient in most cases, although this increase was less than half of what was predicted e.g. for configuration $02\alpha0$, the increase was 0.11% instead of 0.41%.

Configurations $02\alpha30$'s, $02\alpha45$'s and $02\alpha60$'s results differ from the previously mentioned ones but nonetheless were similar to one another. As the angle between the TLD and the acting excitation increased, the distance between the resonant frequencies fell, which indicates a miss-tuning of the TLD.

The behaviour of the liquid near the lower resonant frequency was kept as previously described, with the formation of two waves along the excited main axis and with the addition of one wave in the other main axis at resonance. The variation of this resonant frequency location was similar to what was noticed in the tests performed with just the reservoir.

The lowering of the higher resonant frequency was greater than what was expected from the tests with just the reservoir. Specifically for $02\alpha60$ configuration, the liquid behaviour changed unexpectedly near its higher resonance. Starting in the frequency 0.80 Hz, the water movement left the main axes, starting to move diagonally from one corner of the reservoir to the opposite one and, when the frequency was increased to 0.86 Hz, the water movement changed to the main axis it was not aligned before.

In these configurations, the structure response became more asymmetrical, with a higher response in the lower resonance when compared to the previous configurations and a lower response in the higher one, with the exception of $02\alpha45$ in which case both responses were lowered (although the reduction in the response for the higher resonance was greater). This indicates a positive miss tuning of the TLD, taking into account the study performed by Sun (1991), which would mean that the sloshing frequency increased when compared to the structure.

The variation of the damping coefficient for configuration $02\alpha30$ was pretty much the same as for the previous tests. Configuration $02\alpha45$ results were different, with no major variation on the lower resonance damping and a slight increase in the higher resonance. Configuration 02α60 had a slight increase in damping for the lower resonance and an unexpected decrease for the higher one.

Given the substandard results a new set of tests was scheduled in order to improve the attenuation caused by the TLD. As mentioned in Sections 2.2.5 and 2.2.6, both the ratio of masses and the liquid depth ratio have a significant impact on the damping provided by a TLD. Therefore

This new set of tests was performed keeping the structure and the base displacement caused by the shaking table the same, but reducing the height of the water in order to reduce both ratios, which should increase the performance of the TLD, given that the liquid depth ratio was above the ideal point in the previous tests.

In order to comply with the new stipulations and to keep the reservoir tuned to the structure, it was decided to rotate it 90º as in the previous tests it was apparent that the resonant frequency of the reservoir with the same height of water was higher when its length was smaller.

In this new configuration (denoted as 03α90), the length of the TLD is 40 cm and its width 60 cm. Utilising Equation 9 to determine the height of water to be used in order to tune it to the structure the result is:

$$0.698 = \frac{1}{2\times\pi} \times \sqrt{\frac{\pi\times 9.81}{0.4} \times tanh(\frac{\pi\times h_f}{0.4})} \Leftrightarrow h_f = 0.0325\, m$$

Figure 4.2.12 - Small scale structure with the rectangular reservoir in configuration 03α90.

With this information, the ratio of masses and the liquid depth ratio can be determined as per Equations 16 and 17, respectively:

$$\mu = \frac{4\times 6\times 0.325}{(4\times 28.08)+12.25+9.50+(6\times 7.15)} = 4.41\% \qquad \varepsilon = \frac{3.25}{40/2} = 0.16$$

As can be seen, the ratio of masses fell to a little below 5% and the liquid depth ratio got closer to 0.1 and mostly important below 0.2. This should reflect on better results on the control of the structure displacement.

It should be noted however that there were two problems in the execution of these tests that will impact the results.

The first one was that the new height of water required for the tunning of the TLD was on the limit of the liquid level sensor measuring range, which resulted in some of the results collected by this sensor to be unusable.

The second one was that a beating was present in all tests performed on the new configuration, usually in the intermediary frequencies (from 0.68 Hz to 0.76 Hz). This was visually noticeable and was also perceived in the collected data, but, most importantly, it caused a third displacement peak to appear near the 0.69 Hz frequency.

After applying the FFT to the collected data, the most prominent peaks were at a frequency that was a multiple of the acting frequency, but there was more noise than usual close to this point which is most likely the cause for the beating, probably due to a slight miss-tuning of the TLD.

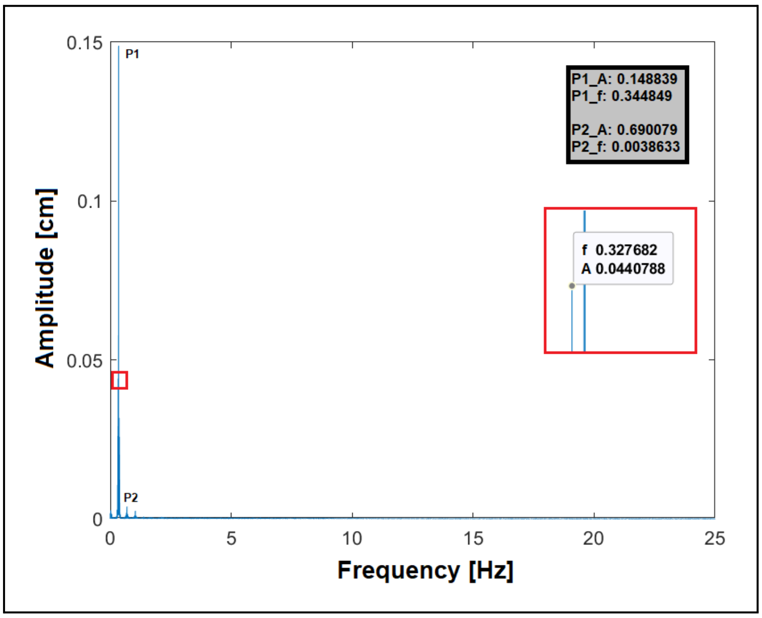

Figure 4.2.13 - Results of the FFT for the structure displacement measurements in configuration 03α90 at frequency 0.69 Hz.

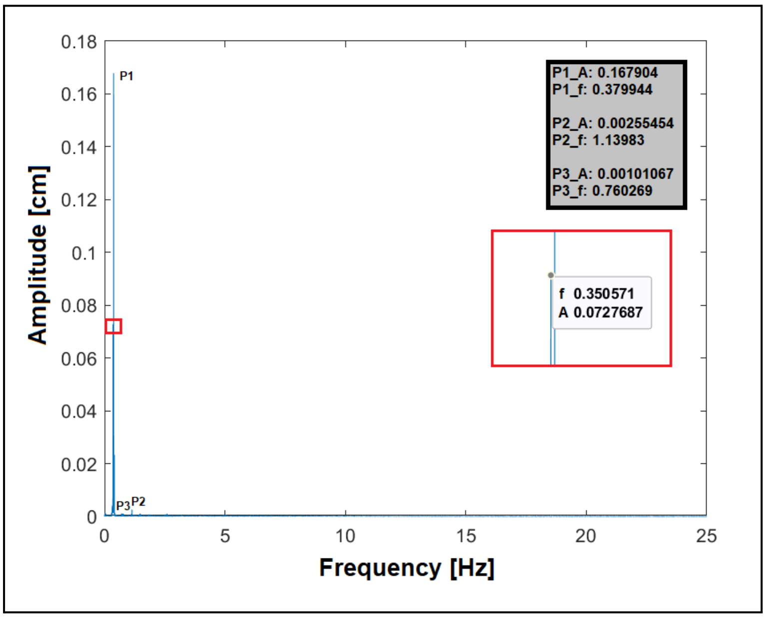

Figure 4.2.14 - Results of the FFT for the structure displacement measurements in configuration 03α90 at frequency 0.76 Hz.

Although these conditions are not ideal, the results of the tests were kept in this study for two reasons: the first one being that a "miss-tuned" TLD should perform worse than a "well-tuned" one (and, as will be demonstrated by results, the new configuration was more effective than any of the older ones) and the second being that most of the data collected by the liquid level sensor was still usable and therefore useful for comparing the expected damping increase to the measured damping coefficient.

Having these constraints in mind, this section will now cover the finer details of the newer tests, as well as their results.

The tests were performed in a similar manner to the previous ones, covering the same frequency range and utilising discrete points (0.02 Hz apart or 0.01 Hz apart while near the resonant frequency) each of which was excited for 10 minutes in order to determine the steady state response of the structure.

As it was expected that the structural displacement would be reduced, the proximity sensor was relocated to a position closer to the structure to guarantee a greater resolution in the collected data. This proved to be a good decision as, with the new configuration, the displacements were reduced to less than half of those measured in the previous tests. As can be clearly seen on Figure 4.2.16.

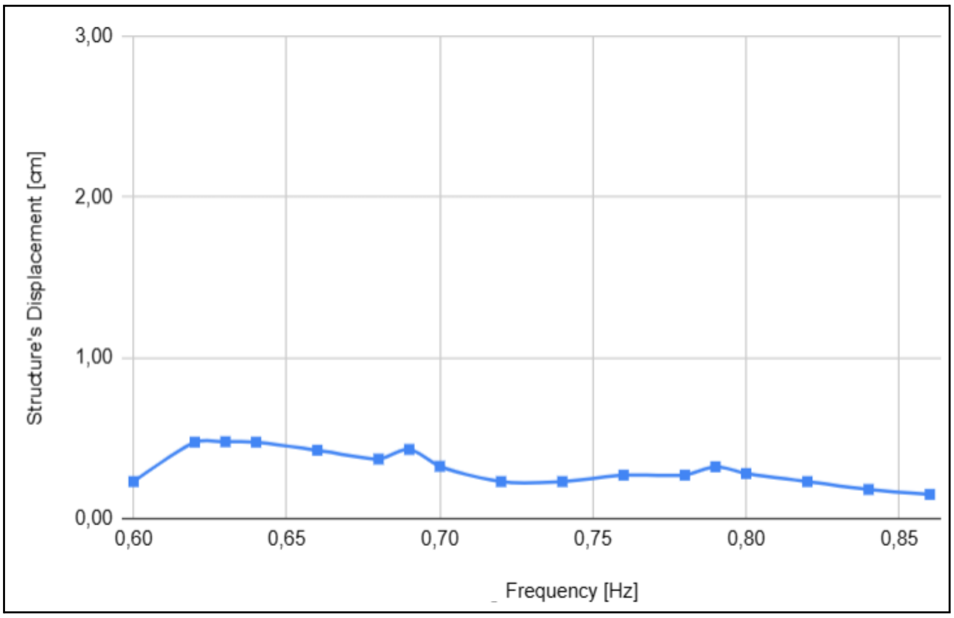

Figure 4.2.15 - Frequency-response of the system in the steady state in configuration 03α90.

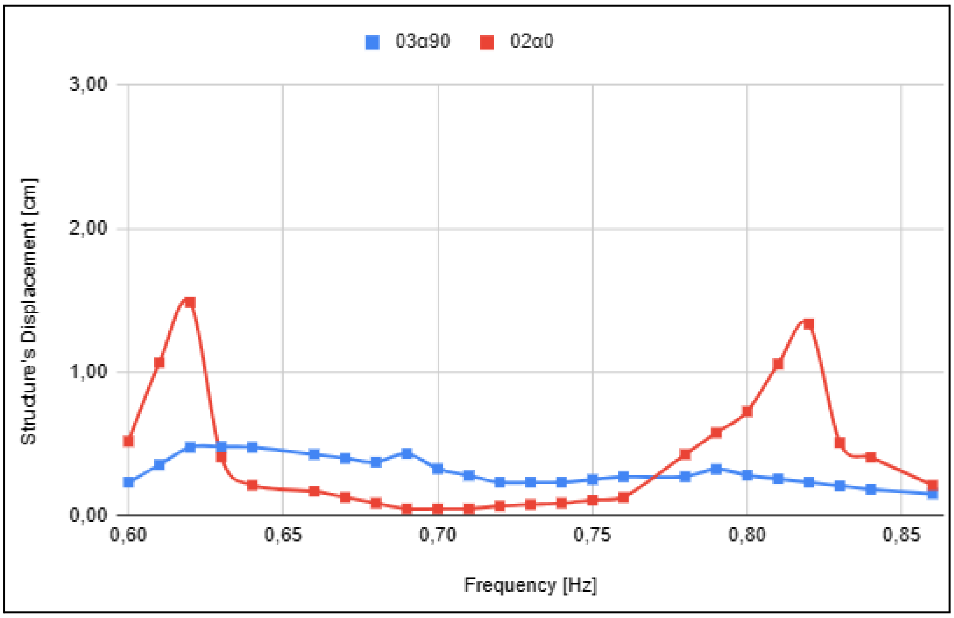

Figure 4.2.16 - Comparison between the responses of the system in configurations 02α0 and 03α90.

The lower resonance occurred at frequency 0.63 Hz and the higher one was at frequency 0.79 Hz. It is also possible to see a third displacement peak at frequency 0.69 Hz caused by the beating interference.

As was noticed in the previous tests, the behaviour of the water in the lower frequencies indicated the formation of two waves, but the occurrence of a third wave on the other main axis shifted from the lower resonance to 0.69 Hz. It was also noted that starting at frequency 0.82 Hz, the water movement left the main axes in similar fashion to what happened in configuration 02α60, although a complete axis shift did not occur in the measured interval.

Due to the smaller structural displacement, it was decided that further investigation should be performed. Three other configurations were studied with the height of water kept the same but with a rotation of the TLD. As it was clear that small rotations had a small impact on the results, only the higher ones were studied, namely 30º, 45º and 60º (utilising the same reference as in the previous tests).

Table 4.2.5 - Information about the tests with the rectangular TLD for its new configurations and the small scale structure

Test ID	Excitation angle to the longer side of the TLD	Height of water [cm]	Base displacement amplitude [mm]
03α90	90º	3.25	0.50
03α60	60º	3.25	0.50
03α45	45º	3.25	0.50
03α30	30º	3.25	0.50

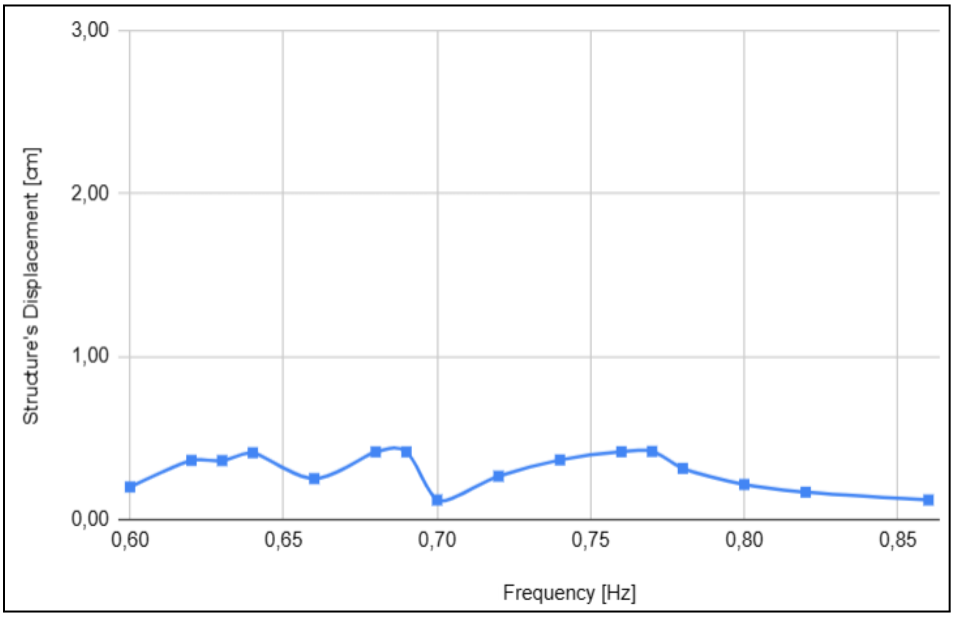

Figure 4.2.17 - Frequency-response of the system in the steady state in configuration 03α60.

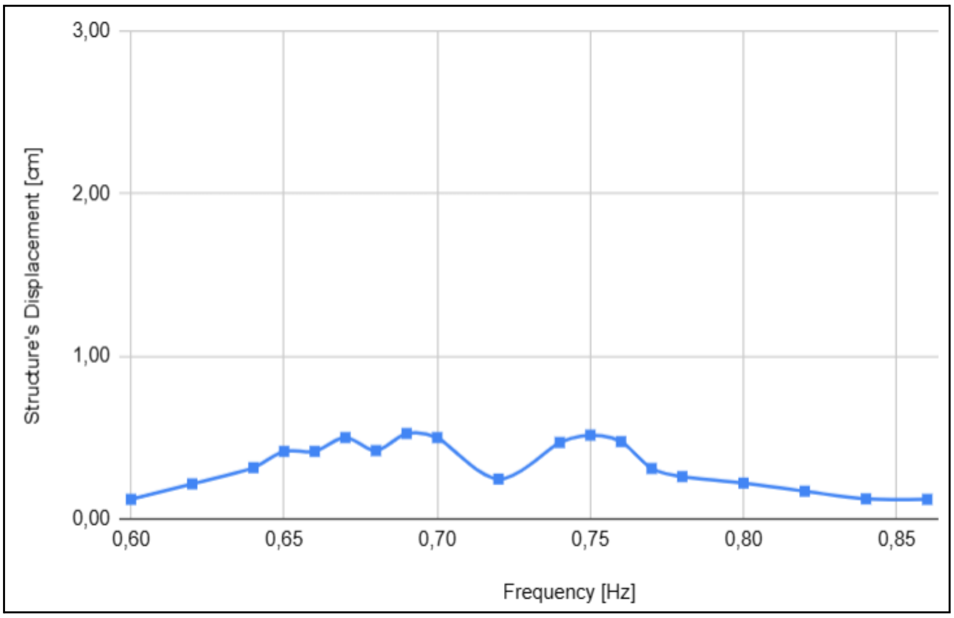

Figure 4.2.18 - Frequency-response of the system in the steady state in configuration $03\alpha45$.

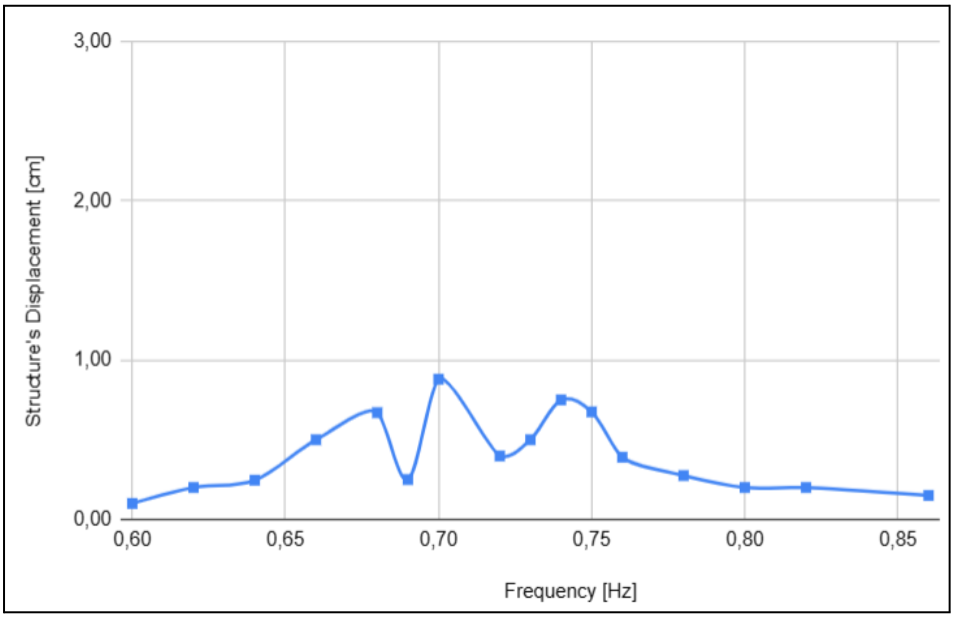

Figure 4.2.19 - Frequency-response of the system in the steady state in configuration $03\alpha30$.

Table 4.2.6 - Results of tests with the rectangular TLD for the new configurations with the excitation frequency at their lower resonant frequency

Test ID	Resonant frequency [Hz]	Liquid surface elevation [cm]	Damping of liquid motion [rad/s]	Expected damping increase	Structure's displacement [cm]	System's damping coefficient
03α90	0.63	0.35	0.0333	0.42%	0.48	0.86%
03α60	0.64	-	-	-	0.41	1.06%
03α45	0.67	0.20	0.0359	0.42%	0.50	1.38%
03α30	0.68	0.55	0.0328	0.38%	0.67	0.87%

Table 4.2.7 - Results of tests with the rectangular TLD for the new configurations with the excitation frequency at their higher resonant frequency

Test ID	Resonant frequency [Hz]	Liquid surface elevation [cm]	Damping of liquid motion [rad/s]	Expected damping increase	Structure's displacement [cm]	System's damping coefficient
03α90	0.79	-	-	-	0.32	0.85%
03α60	0.76	1.00	0.0310	0.32%	0.42	0.50%
03α45	0.75	1.00	0.0307	0.33%	0.52	0.66%
03α30	0.74	1.15	0.0295	0.32%	0.75	0.81%

When compared to the previous tests, the newer results demonstrate that these new configurations are more adequate for the control of the structure in question. With the structural displacements being in general lower and the damping coefficients being in general higher.

These results were also more in line to what was expected from the initial assumptions, with the TLD performing better when its main axis is aligned with the movement of the structure (configuration 03α90) with a decrease in the control of the structural displacement whenever the rotation of the TLD increases.

For the new configurations, the attenuation of the structure response in most cases was closer to 80%, which should be reflected in an increase in the damping coefficient by factor of five, which once again was not the case.

The damping coefficient of the system continued to be small and different from what was expected from the analytical method based on the damping of liquid motion, although the result were better than what was expected for the lower resonance, with more variation for the higher one with the results from configurations 03α60 and 03α45 underperforming and, for configuration 03α30, the results being close to what was expected. However, Even the worst performing configurations provided a similar damping to the previous tests, which presents an improvement all around even with the occurrence of the beating.

4.3: Interaction of the ring cell TLD with the small scale structure

This section will cover the tests performed with the ring cell reservoir acting as the TLD on the small scale structure. Due to the inconsistency of the predicted results reached through equations 12 and 14 in the previous tests, this analysis was dropped in this phase of the work as it was deemed that their results for a non-ideal case would prove unsubstantial.

Similarly to what was previously done, a sweep frequency test utilising discrete points (0.02 Hz apart or 0.01 Hz apart while near the resonant frequency) each of which was excited for 10 minutes in order to determine the steady state response of the structure. As it is believed that the behaviour of the ring cell TLD will be similar to that of a rectangular one and the cell has a similar size to the previously studied TLD, it was decided to keep the same frequency interval (0.60 Hz to 0.86 Hz).

Six configurations were studied for this reservoir, in order to fully cover all positions a cell could assume inside the annular TLD. Table 4.3.1 contains the conditions in which each configuration test was performed.

Table 4.3.1 - Information about the tests with the ring cell TLD and the small scale structure

Test ID	Excitation angle to the centre of the ring cell TLD	Height of water [cm]	Base displacement amplitude [mm]
04α0	0º	3.7	0.50
04α18	18º	3.7	0.50
04α36	36º	3.7	0.50
04α54	54º	3.7	0.50
04α72	72º	3.7	0.50
04α90	90º	3.7	0.50

Figure 4.3.1 - Small scale structure with the ring cell reservoir in configuration $04\alpha0$.

Visual observation of the sloshing of the water inside the ring cell reservoir showed that it flowed radially (as if it had started on the centre point of the ring) for most configurations with no major disturbance until the resonance was reached. For the lower frequencies the formation of two waves was noticed as was the case for the previous tests and no axis shift occurred. For configuration $03\alpha90$ only, the water flowed from the reservoir's straight sides (i.e. aligned with the movement of the pendulum) similarly to its behaviour in the rectangular TLD. There was no noticeable wave breaking in any of the tests covered in this section.

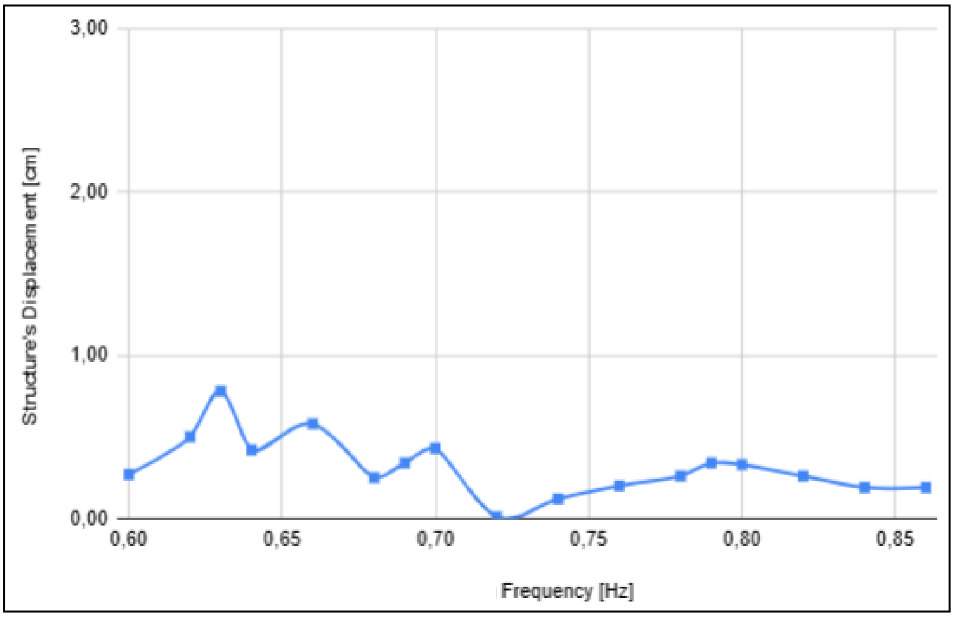

Figure 4.3.2 - Frequency-response of the system in the steady state in configuration $04\alpha0$.

Given the assumption that the ring cell will behave like a rectangle, configuration 04α0 should perform similarly to configuration 03α90, due to the similarities between both tests. This seemed to be the case as can be seen in Figure 4.3.3.

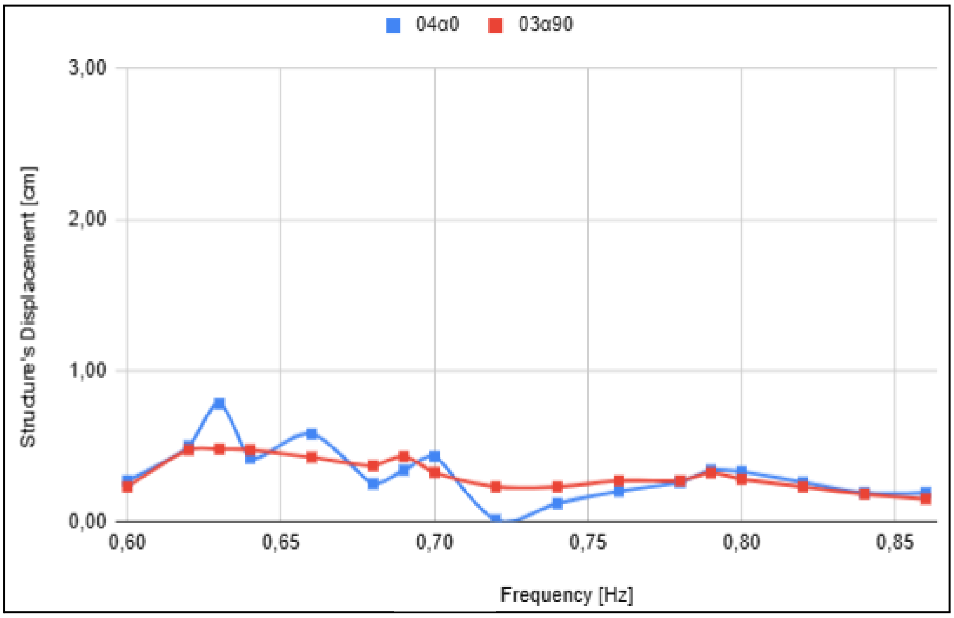

Figure 4.3.3 - Comparison between the responses of the system in configurations 04α0 and 03α90.

Both systems' resonant frequencies were equal, with the lower resonance at 0.63 Hz and the higher one at 0.79 Hz and with the presence of beating, although, for configuration 04α0 this occurred at the range 0.66 Hz to 0.69 Hz, while for configuration 03α90 it occurred at frequencies 0.68 Hz to 0.76 Hz, as previously mentioned.

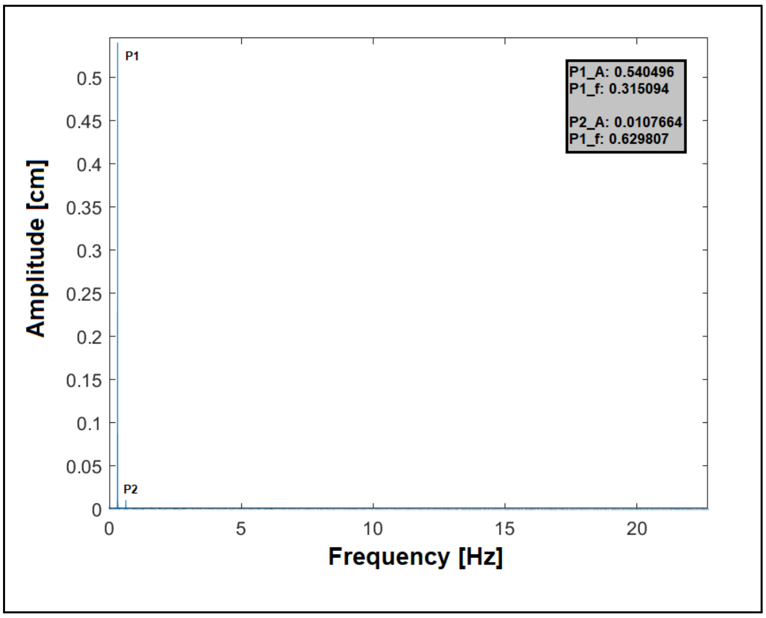

Figure 4.3.4 - Results of the FFT for the structure displacement measurements in configuration $04\alpha0$ at frequency 0.63 Hz.

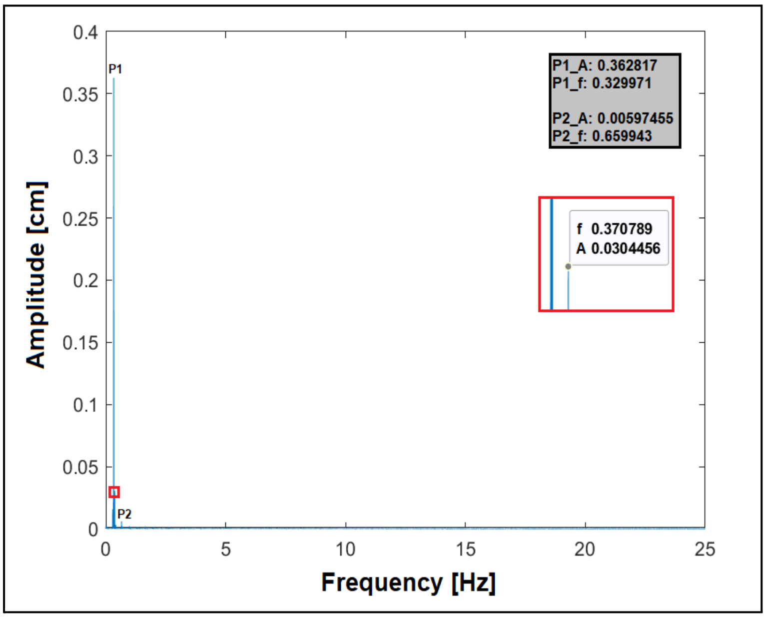

Figure 4.3.5 - Results of the FFT for the structure displacement measurements in configuration $04\alpha0$ at frequency 0.66 Hz.

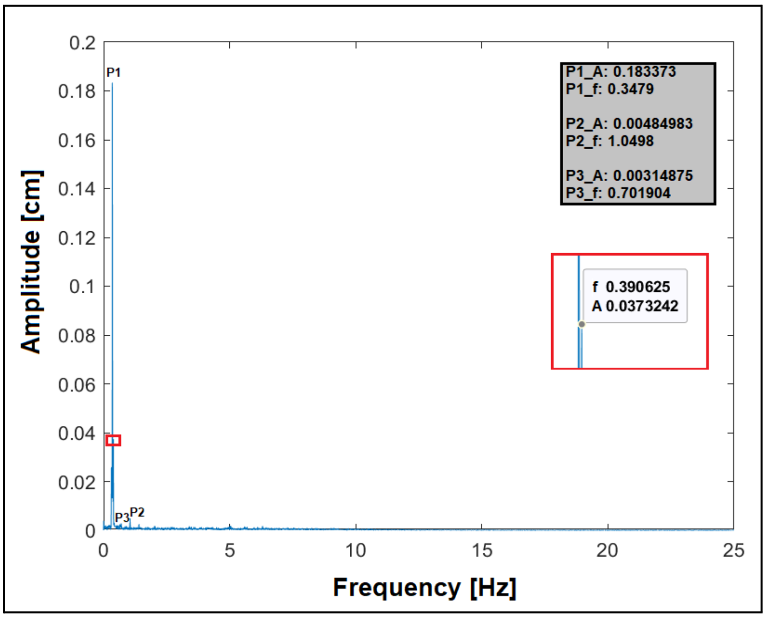

Figure 4.3.6 - Results of the FFT for the structure displacement measurements in configuration 04α0 at frequency 0.70 Hz.

Configuration 03α90 performed better at the lower end of the studied frequency interval. Configuration 04α0 provided a displacement attenuation of 71% compared to 03α90's 82%. The displacement peak caused by the beating was slightly higher for 04α0 as well. That being said, the ring cell TLD still had a good performance, although, due to the asymmetry of the graph a slight positive miss-tune might be in effect.

In order to have all the information required to make predictions about the behaviour of the quarter-ring TLD, tests were made for configuration 04α90, although it was expected that the TLD would be severely miss-tuned to the structure and therefore provide little damping. As shown in Figure 4.3.7, this was indeed the case.

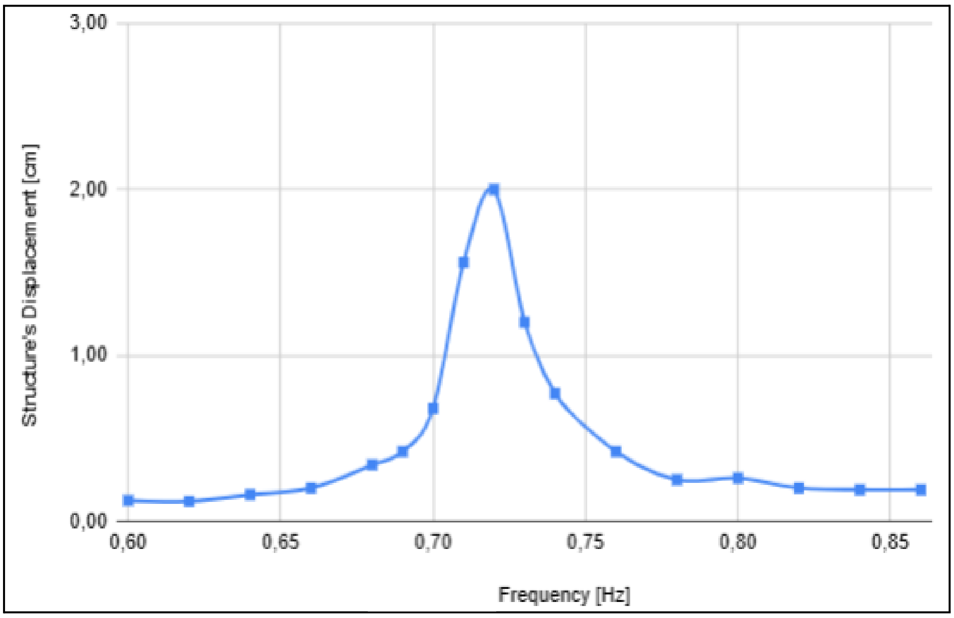

Figure 4.3.7 - Frequency-response of the system in the steady state in configuration 04α90.

In this configuration, the resonance occurred at frequency 0.72 Hz, with the formation of only one peak of displacement that, when compared to the results of configuration 04α0, was very pronounced, reaching 2 cm. This means that the displacement attenuation was only 20%. This was expected as the TLD in this configuration is not tuned to the structure.

Moving on to configurations 04α18, 04α36, 04α54 and 04α72, the performance of the TLD fell in between the others mentioned in this section. As the angle between the excitation and the centre of the TLD increased, the peaks became more pronounced and the resonance tended towards 0.72 Hz. Figures 4.3.5, 4.3.6, 4.3.7 and 4.3.8 contain the frequency-response curves for the latter configurations and Tables 4.3.2 and 4.3.3 display the results for all tests with the ring cell TLD.

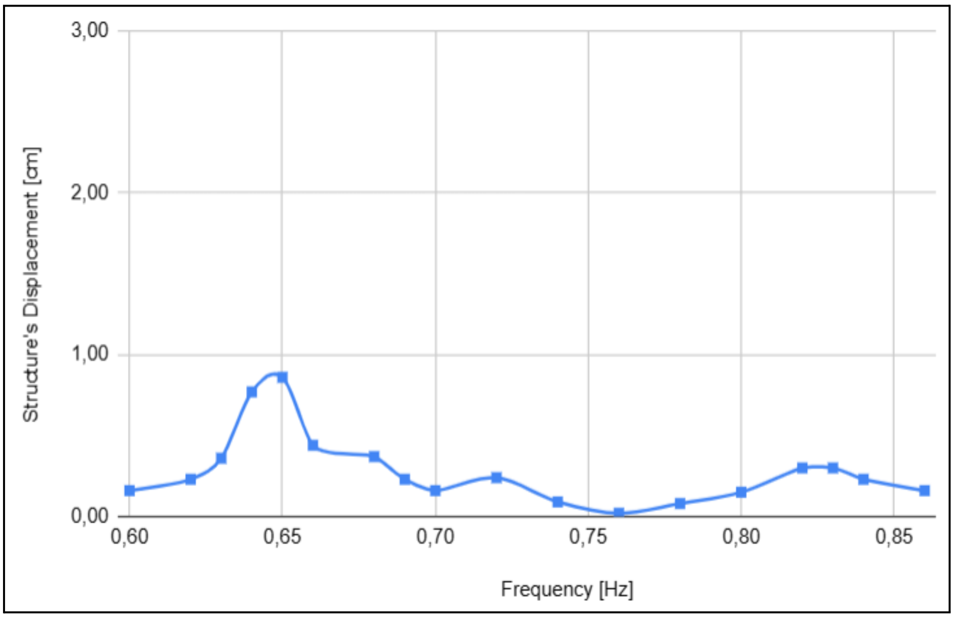

Figure 4.3.8 - Frequency-response of the system in the steady state in configuration $04\alpha18$.

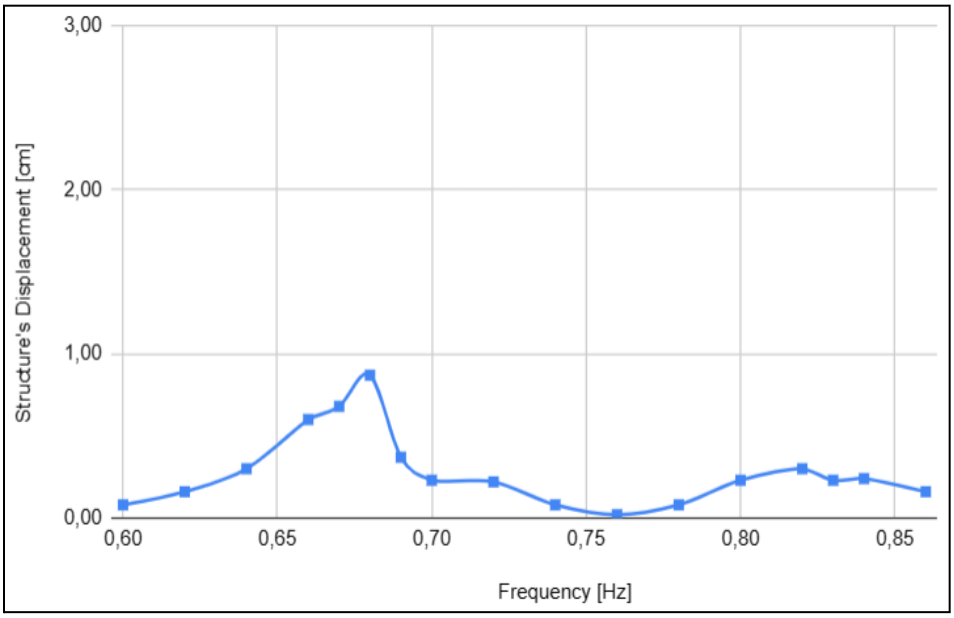

Figure 4.3.9 - Frequency-response of the system in the steady state in configuration $04\alpha36$.

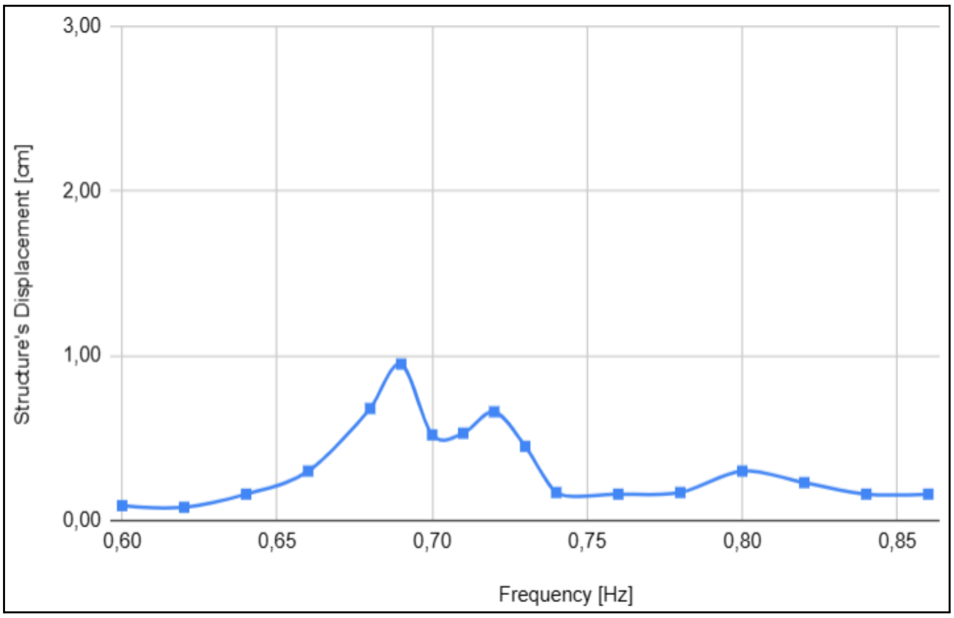

Figure 4.3.10 - Frequency-response of the system in the steady state in configuration $04\alpha54$.

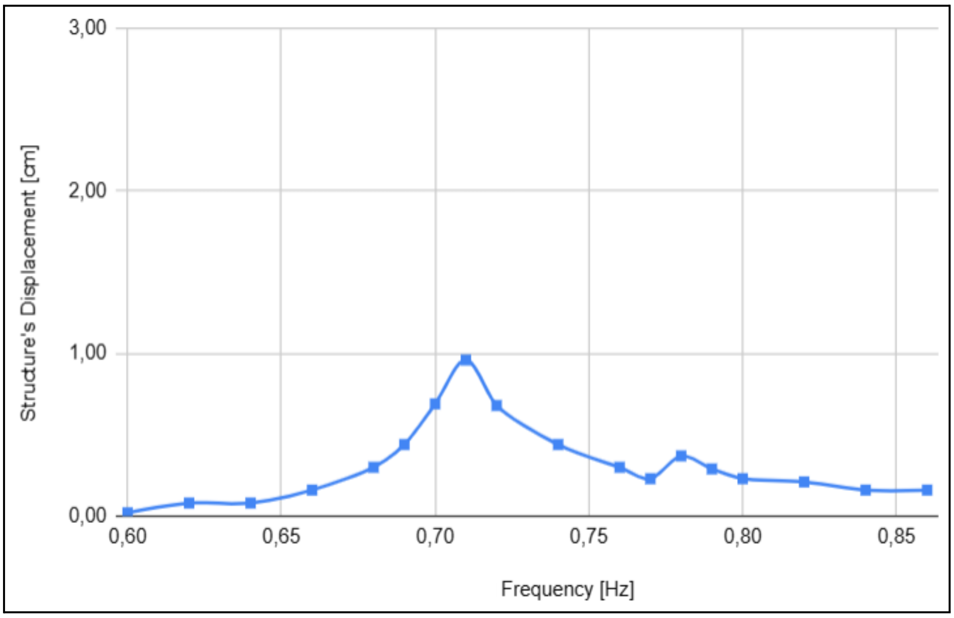

Figure 4.3.11 - Frequency-response of the system in the steady state in configuration $04\alpha72$.

Table 4.3.2 - Results of tests with the ring cell reservoir for the multiple configurations with the excitation frequency at their lower resonant frequency

Test ID	Resonant frequency [Hz]	Liquid surface elevation [cm]	Structure's displacement [cm]	System's damping coefficient
04α0	0.63	0.94	0.78	0.74%
04α18	0.65	1.52	0.86	0.43%
04α36	0.68	1.53	0.87	0.99%
04α54	0.69	1.30	0.95	0.95%
04α72	0.71	1.63	0.96	0.99%
04α90	0.72	2.70	2.00	0.47%

Table 4.3.3 - Results of tests with the ring cell reservoir for the multiple configurations with the excitation frequency at their higher resonant frequency

Test ID	Resonant frequency [Hz]	Liquid surface elevation [cm]	Structure's displacement [cm]	System's damping coefficient
04α0	0.79	1.74	0.34	0.45%
04α18	0.83	0.48	0.30	0.91%
04α36	0.82	0.29	0.30	1.05%
04α54	0.80	0.25	0.30	1.30%
04α72	0.78	0.10	0.37	1.48%

As can be seen, all configurations that had two peaks were asymmetrical, with the displacement peak at the lower resonance frequency being more pronounced, which can be an indicator of positive miss-tuning. As mentioned before, there was an increase of the response at the lower resonant frequency, but there was no significant variation of the response at the higher one.

Configurations 04α0, 04α36, 04α54 and 04α72 had the occurrence of beatings although only configurations 04α0 and 04α54 had more than one frequency where this happened and, with the exception of configuration 04α36, the beatings were always off the resonance. The beating position on the frequency spectrum changed with the increase of the rotation, from 0.66 Hz to 0.69 Hz for configuration 04α0; to 0.68 Hz for 04α36; to 0.71 Hz to 0.73 Hz and 0.76 Hz for 04α54; and to just 0.76 Hz for04α72.

The damping coefficient of the system varied inconsistently, but, with exception of configurations 04α0 higher resonance, 04α18 lower resonance and, as expected, 04α90, there was a major relative increase on the damping throughout, more than doubling in most cases.

The attenuation of the response at the lower resonance was, as mentioned before, 71% for configuration 04α0 and 20% for 04α90. The other configurations' attenuations varied from 68% to 64%, being as expected a little less effective than the first configuration.

4.4: Interaction of the ring cell TLD with the big scale structure

Initial tests with just the pendulum were performed to confirm its natural frequency. Initially, the pendulum was excited until it reached a steady state of movement at the expected (due to the tests performed with the small scale model) resonant frequency of 0.69 Hz. Once the excitation was stopped, the structure entered free vibration, with the displacement decaying at a rate equal to its natural frequency, in this case approximately 0.68 Hz. This represents a 3% reduction of the expected frequency obtained through the analytical method, which is acceptable.

Once this was determined, a sweep frequency test utilising discrete points was performed with the structure being excited for 20 minutes (it was noticed that due to the greater mass of the structure, the transitory response remained in effect for a longer period of time) in order for it to reach its steady state response. These tests were performed with two base displacement amplitudes, namely 0.5 mm and 0.25 mm. Higher base amplitudes were also studied but, to preserve the integrity of the pendulum, it was decided only those two displacement amplitudes would be further investigated.

Figures 4.4.1 and 4.42 contain the frequency-response curves of the pendulum with the higher and lower base displacement amplitudes, respectively.

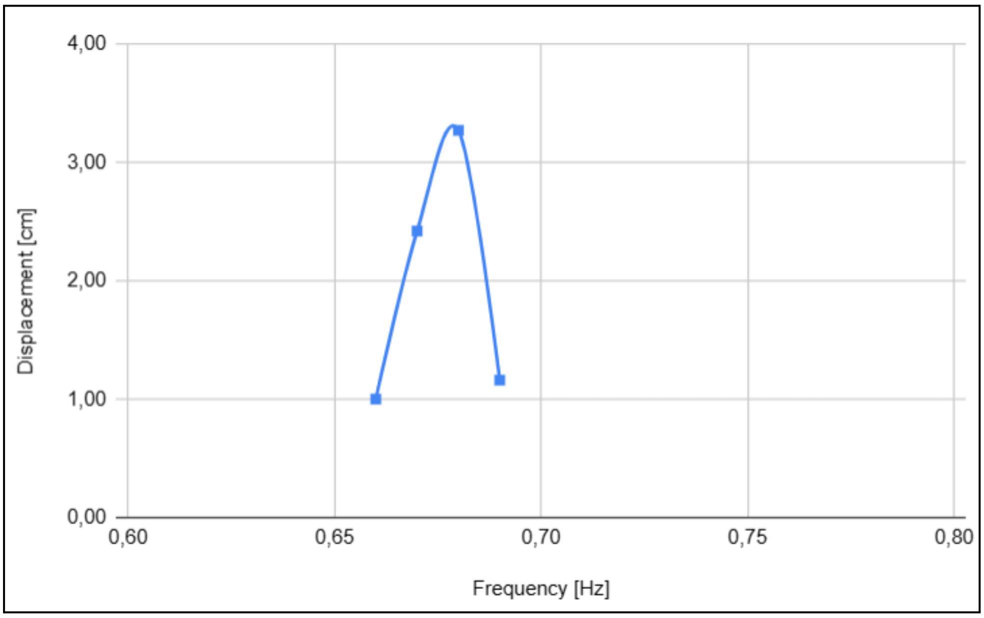

Figure 4.4.1 - Frequency-response of the bigger pendulum in the steady state with the higher base displacement.

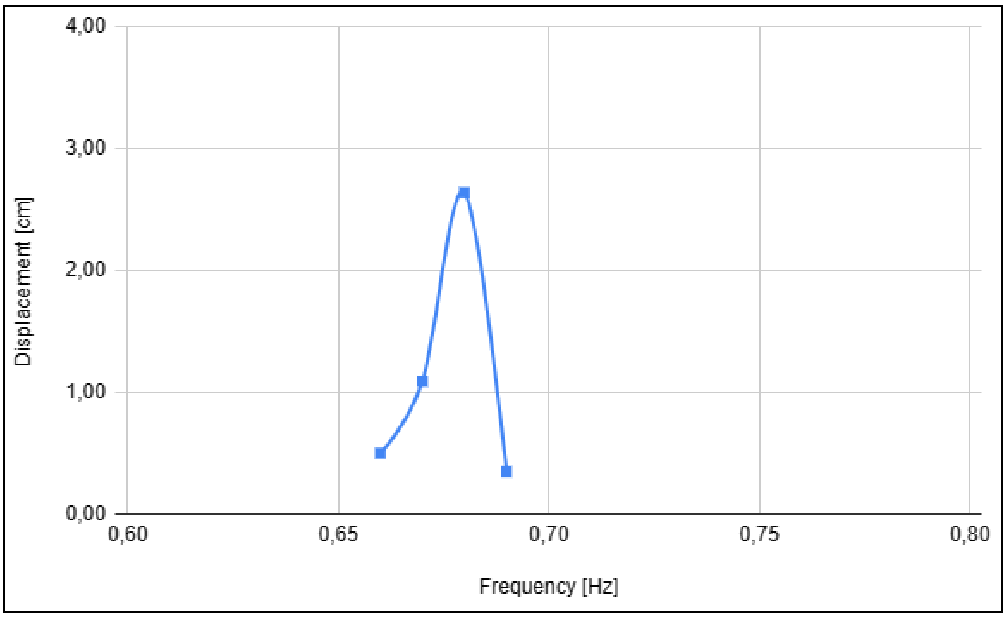

Figure 4.4.2 - Frequency-response of the bigger pendulum in the steady state with the lower base displacement.

With the natural frequency of the pendulum and its maximum steady state response determined, it was possible to calculate its damping coefficient through the decay of the free vibration until it reached 50% of the maximum response.

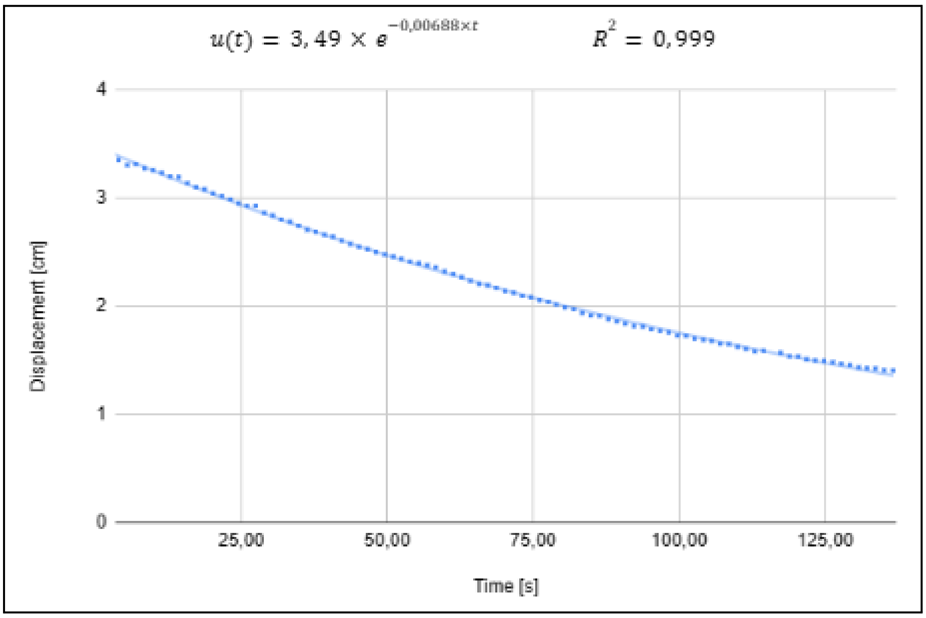

Figure 4.4.3 - Decay of free vibration of the bigger pendulum starting at its steady state response for the higher base displacement.

$$u(t) = 3.49 \times e^{-0.0068 \times t} \Leftrightarrow$$

$$\Leftrightarrow e^{-\xi \times \omega \times t} \times [u_o \times cos(\omega_d \times t) + \frac{u'_o + u_o \times \xi \times \omega}{\omega_d} \times sen(\omega_d \times t)] = 3.49 \times e^{-0.00688 \times t} \Leftrightarrow$$

$$\Leftrightarrow - \xi \times 0.68 \times t = - 0.00688 \times t \Leftrightarrow \xi = 0.16\%$$

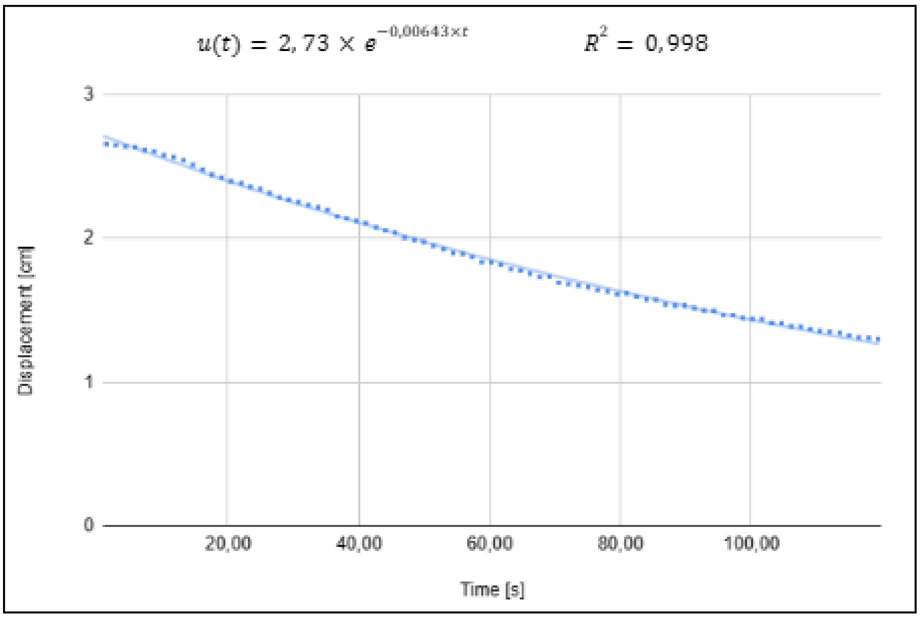

Figure 4.4.4 - Decay of free vibration of the bigger pendulum starting at its steady state response for the lower base displacement.

$$u(t) = 2.73 \times e^{-0.00643 \times t} \Leftrightarrow$$

$$\Leftrightarrow e^{-\xi \times \omega \times t} \times [u_o \times cos(\omega_d \times t) + \frac{u'_o + u_o \times \xi \times \omega}{\omega_d} \times sen(\omega_d \times t)] = 2.73 \times e^{-0.00643 \times t} \Leftrightarrow$$

$$\Leftrightarrow - \xi \times 0.68 \times t = - 0.00643 \times t \Leftrightarrow \xi = 0.15\%$$

Table 4.4.1 - Results of tests with the bigger pendulum

Base displacement amplitude [mm]	Oscillation frequency [Hz]	Structure's displacement [cm]	Structure's damping coefficient
0.50	0.68	3.27	0.16%
0.25	0.68	2.64	0.15%

The behaviour was similar to that of the small scale model, with a relatively high structure displacement despite the small base displacement and an insignificant damping coefficient, both of these metrics were more accentuated in this case, however. The response in the resonance for the different base displçacement amplitudes is significant, a variation of 20% of the displacement in the resonance and upwards of 50% for the other frequencies.

With this information in mind, the tests with the ring cell TLD were performed. Table 4.4.2 contains the conditions in which each test was performed.

Table 4.4.2 - Information about the tests with the ring cell TLD and the big scale structure

Test ID	Excitation angle to the centre of the ring cell TLD	Height of water [cm]	Base displacement amplitude [mm]
$05\alpha0a50$	0º	3.5	0.50
$05\alpha0a25$	0º	3.5	0.25

The height of water was defined through Equation 9, with this parameter, through Equations 16 and 17, the ratio of masses and the liquid depth ratio can be calculated.

$$0.68 = \frac{1}{2\times\pi} \times \sqrt{\frac{\pi\times9.81}{0.426} \times tanh(\frac{\pi\times h_f}{0.426})} \Leftrightarrow h_f = 0.035\ m$$

$$\mu = \frac{8}{12+50+35+816+78+7.22} = 0.81\% \qquad \varepsilon = \frac{3.5}{42.6/2} = 0.16$$

Figure 4.4.5 - Big scale structure with the ring cell reservoir in configurations $05\alpha0a50$ and $05\alpha0a25$.

In these tests there were occurrences of wave breaking, more pronounced when the base displacement was higher and near the resonances, but still noticeable in the other frequencies. Figures 4.4.6 and 4.4.7 and Table 4.4.3 contain the results of the tests.

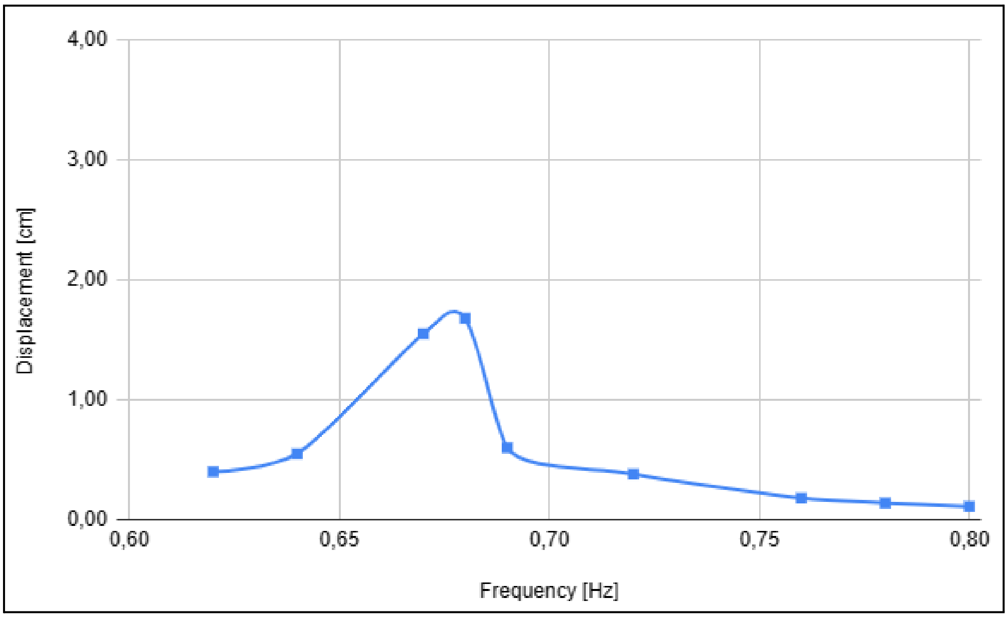

Figure 4.4.6 - Frequency-response of the system in the steady state in configuration $05\alpha0a50$.

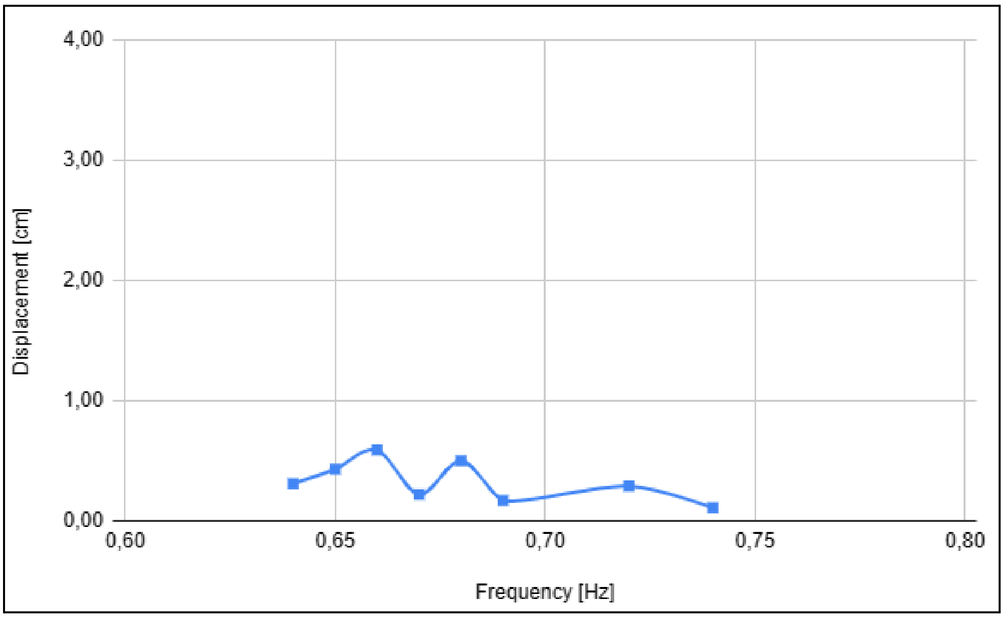

Figure 4.4.7 - Frequency-response of the system in the steady state in configuration $05\alpha0\alpha25$.

Table 4.4.3 - Results of tests with the ring cell TLD for the multiple configurations at their resonances

Test ID	Resonant frequency [Hz]	Structure's displacement [cm]	System's damping coefficient
$05\alpha0\alpha50$	0.68	1.68	1.26%
$05\alpha0\alpha25$	0.66	0.59	1.38%
$05\alpha0\alpha25$	0.72	0.29	1.80%

Both tests showed a noticeable attenuation of the structure displacement, nearly 50% for configuration $05\alpha0\alpha50$ and nearly 80% for configuration $05\alpha0\alpha25$ lower resonance. The behaviour of the structure varied greatly between both tests with the formation of a pronounced single peak when the base displacement was higher and two peaks when the base displacement was lower, with the lower peak being more pronounced (with displacements twice as big). Beatings were noticeable in both tests, although, for configuration $05\alpha0\alpha50$, it only happened in frequency 0.72 Hz, while, for configuration $05\alpha0\alpha25$, they were noticeable at frequencies 0.68 Hz and 0.72 Hz, with the formation of a third peak at this first frequency.

There was also a sharp increase in damping, with a relative increase of almost eight times for configuration $05\alpha0\alpha50$, and reaching upwards of twelve times for the higher resonance of configuration $05\alpha0\alpha25$. However, the damping coefficient of the structure was still very small in both configurations.

4.5: Interaction of the quarter ring TLD with the big scale structure

This final section will cover the tests performed with the quarter ring reservoir acting as the TLD on the big scale structure for two base displacement amplitudes and for the two rotations, to encompass all positions the internal cells could assume on the annular TLD (considering the symmetric behaviour of the acting cells).

Similarly to what was previously done, a sweep frequency test utilising discrete points (0.02 Hz apart or 0.01 Hz apart while near the resonant frequency) each of which was excited for 10 minutes, as it was determined that, with the presence of a control device, this interval of time was enough for the structure to reach its steady state response.

Table 4.5.1 contains the information about the tests performed with the quarter ting TLD.

Table 4.5.1 - Information about the tests with the quarter ring TLD and the big scale structure

Test ID	Excitation angle to the centre of the ring	Height of water [cm]	Base displacement amplitude [mm]
$06\alpha0a50$	0º	3.5	0.50
$06\alpha0a25$	0º	3.5	0.25
$06\alpha90a50$	90º	3.5	0.50
$06\alpha90a25$	90º	3.5	0.25

For configurations $06\alpha0a50$ and $06\alpha0a25$, due to the observed behaviour of the ring cell reservoir in Section 4.3 and making a comparison with the behaviour of the rectangular reservoir in Sections 4.1 and 4.2, it can be assumed that the behaviour of each cell is going to be very similar in terms of sloshing frequency and liquid depth ratio, as the height of water is constant. Therefore, Equations 18, 19, 20, 21 and 22 will result in the same characteristics of a singular cell with the same height of water (see Section 4.4), therefore:

$$f_0 = \frac{0.68 + 0.68}{2} = 0.68\,Hz \qquad \Delta\gamma = \frac{(0.68 - 0.68)}{0.68} = 0 \qquad \varepsilon_0 = \frac{0.16 + 0.16}{2} = 0.16$$

$$\Delta R = 0 \qquad \beta_i = 0\,Hz$$

The ratio of masses is simply five times that of Section 4.4:

$$\mu = 5 \times 0.81\% = 4.05\%$$

Figures 4.5.1 and 4.5.2 and Table 4.5.2 contain the results for configurations $06\alpha0a50$ and $06\alpha0a25$.

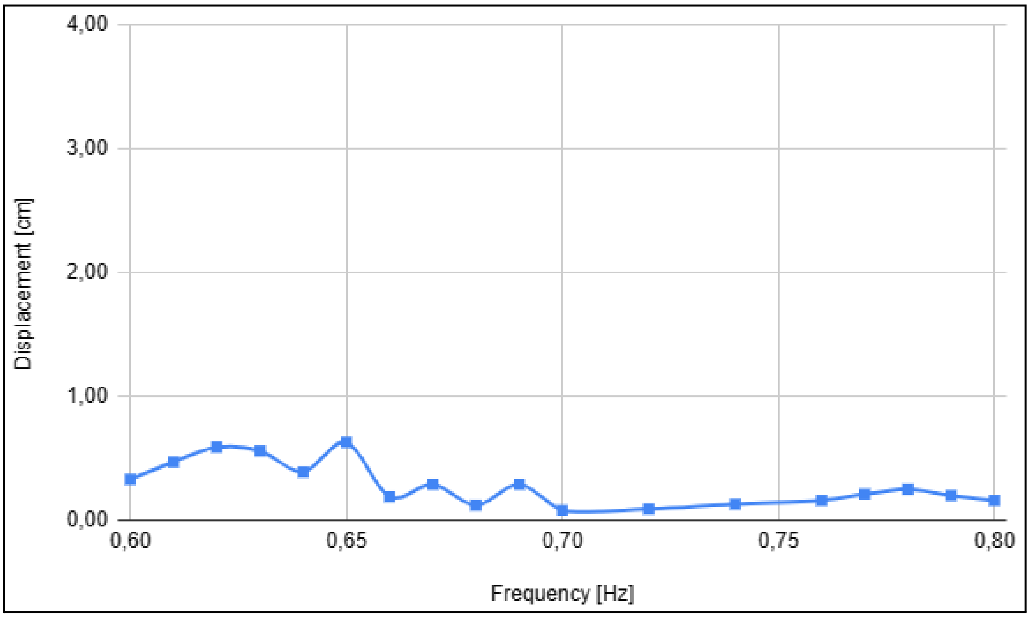

Figure 4.5.1 - Frequency-response of the system in the steady state in configuration $06\alpha0a50$.

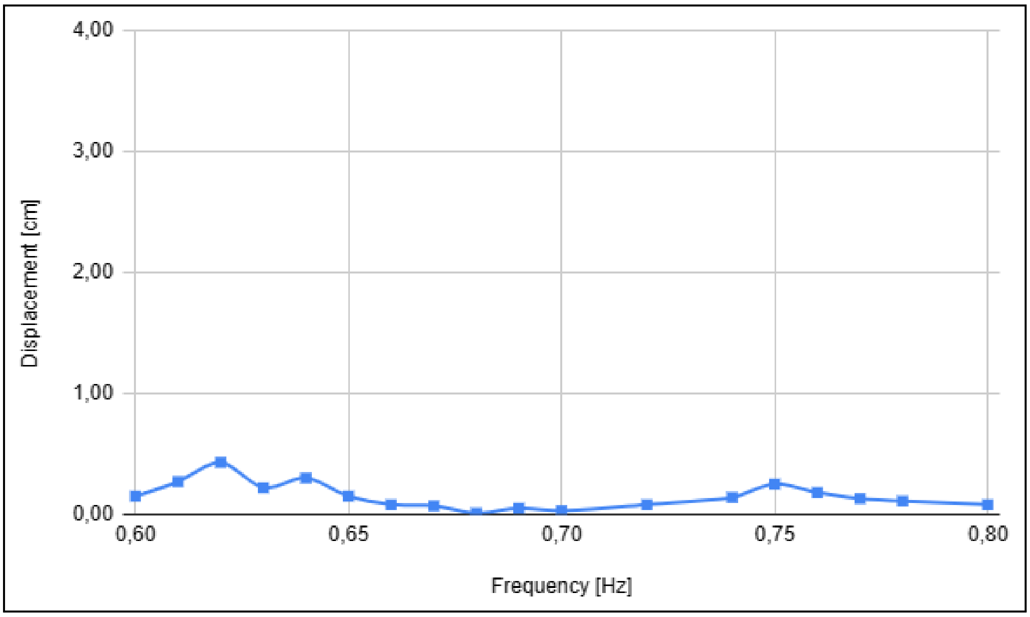

Figure 4.5.2 - Frequency-response of the system in the steady state in configuration $06\alpha0a25$.

Table 4.5.2 - Results of tests with the quarter ring TLD for its main configurations

Test ID	Resonant frequency [Hz]	Structure's displacement [cm]	System's damping coefficient
$06\alpha0a50$	0.65	0.63	1.71%
$06\alpha0a50$	0.78	0.25	1.43%
$06\alpha0a25$	0.62	0.43	0.57%
$06\alpha0a25$	0.75	0.25	0.44%

Both tests showed a great attenuation of the structure displacement, 81% for configuration $06\alpha0a50$ and 84% for configuration $06\alpha0a25$ lower resonances with both higher resonances being barely noticeable, creating an asymmetrical curve, especially in configuration $06\alpha0a50$ where a relatively high displacement plateau formed near frequency 0.62 Hz. This asymmetry was, however, expected from the results with the ring cell reservoir in Section 4.3.

Beatings were noticeable in both tests, for configuration $06\alpha0a50$, they were noticeable at frequencies 0.67 Hz, 0.69 Hz, 0.70 Hz and 0.74 Hz, with the formation of two smaller peaks near the lesser of these four and, for configuration $06\alpha0a25$, they were noticeable at frequencies 0.74 Hz and 0.75 Hz.

There was a sharp increase in damping in both of configuration $06\alpha0a50$'s results, with a nine to 10 times increase in damping. This was not the case for configuration $06\alpha0a25$, where there was a smaller increase of just three to four times. Nonetheless, as was the case for all other tests, the damping coefficient of the structure was still very small.

As for configurations $06\alpha90a50$ and $06\alpha90a25$, the centre cell will have a different sloshing frequency than the rest which should impact the performance of the TLD. Keeping the assumption of a rectangular reservoir, with Equations 9 and 17, it is possible to calculate the sloshing frequency and the liquid depth ratio. The ratio of masses is not altered from the previous tests.

$$f_f = \frac{1}{2\times\pi} \times \sqrt{\frac{\pi\times9.81}{0.551} \times tanh(\frac{\pi\times0.035}{0.551})} = 0.53\,Hz \qquad \varepsilon = \frac{3.5}{55.1/2} = 0.14 \qquad \mu = 4.05\%$$

Therefore, Equations 18, 19, 20, 21 and 22 can be applied to determine the characteristics of the MTLD.

$$f_0 = \frac{0.68 + 0.53}{2} = 0.61\, Hz \qquad \Delta\gamma = \frac{(0.68 - 0.61)}{0.61} = 11\% \qquad \varepsilon_0 = \frac{0.16 + 0.14}{2} = 0.15$$

$$\Delta R = \frac{0.68 - 0.61}{0.68} = 0.10 \qquad \beta_1 = \beta_2 = \beta_4 = \beta_5 = 0\, Hz \qquad \beta_3 = 0.68 - 0.63 = 0.05\, Hz$$

Figures 4.5.3 and 4.5.4 and Table 4.5.3 contain the results for configurations $06\alpha90a50$ and $06\alpha90a25$.

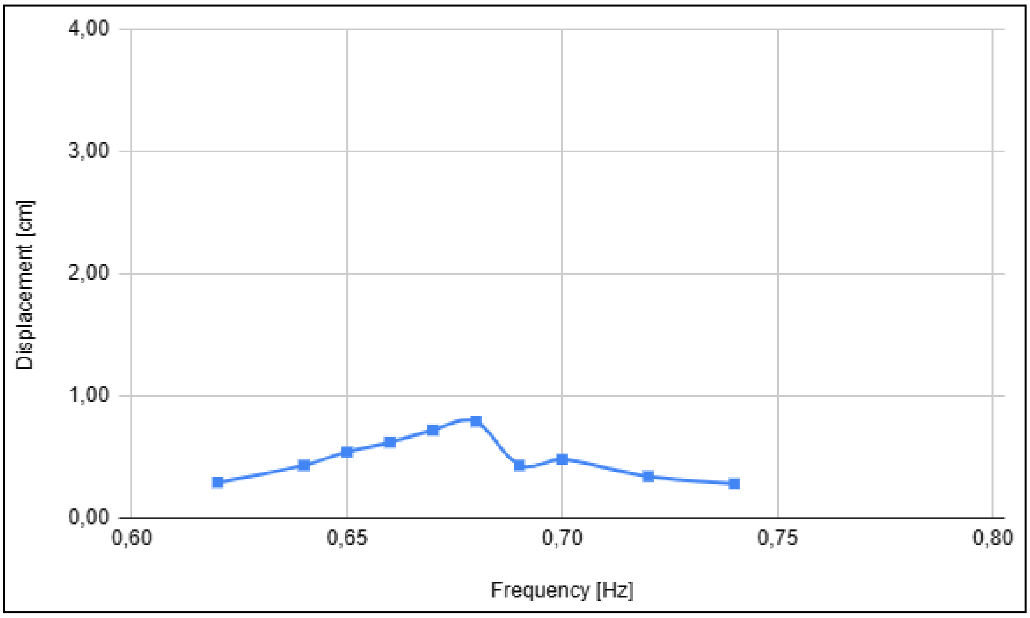

Figure 4.5.3 - Frequency-response of the system in the steady state in configuration $06\alpha90a50$.

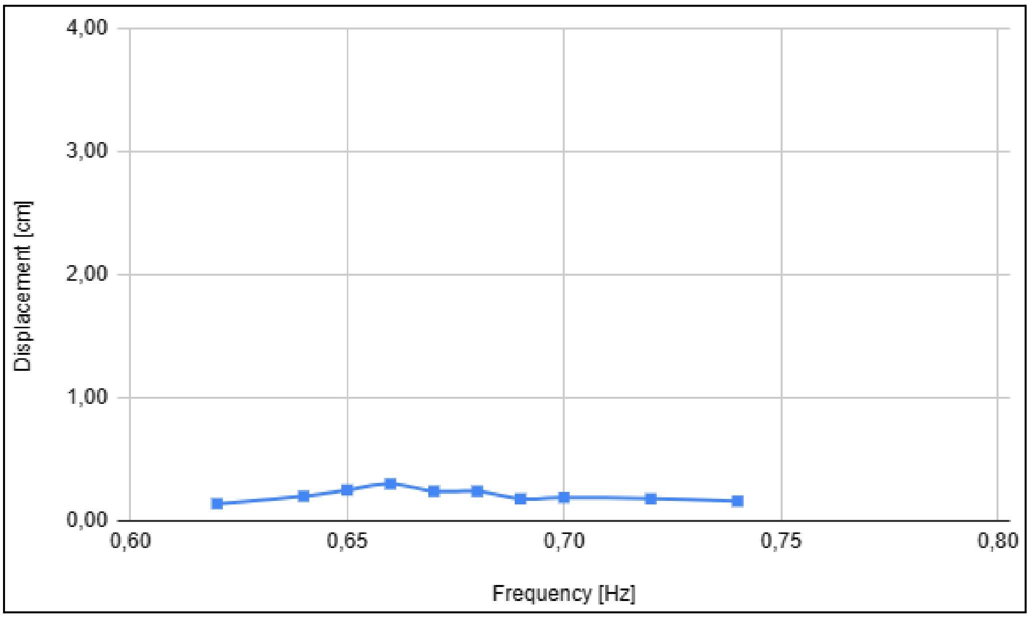

Figure 4.5.4 - Frequency-response of the system in the steady state in configuration $06\alpha90a25$.

Table 4.5.3 - Results of tests with the quarter ring TLD for the configurations with a 90º rotation

Test ID	Resonant frequency [Hz]	Structure's displacement [cm]	System's damping coefficient
$06\alpha90a50$	0.68	0.79	2.55%
$06\alpha90a25$	0.66	0.30	2.22%

The behaviour of the structure in these tests was more comparable to the ones presented in Section 4.4. In configuration $06\alpha90a50$, there was only a single peak and, in configuration $06\alpha90a25$, the structure behaviour was much better, with a barely noticeable resonance. The attenuation reached 76% in configuration $06\alpha90a50$ and 89% in configuration $06\alpha90a25$.

Although the parameters of the MTLD obtained above indicated a miss tuning of 11%, this was not reflected in the results, as there was not a great reduction in the effectiveness of the damper and the occurrence of beating was greatly reduced from the previous tests only being noticeable in configuration $06\alpha90a50$ at a frequency of 0.70 Hz.

And, unexpectedly, the damping coefficient reached its highest values in these tests, with a increase of nearly 16 times for configuration $06\alpha90a50$ and nearly 15 times for configuration $06\alpha90a25$, an increase of nearly 50% and nearly 400% when compared to configurations $06\alpha0a50$ and $06\alpha0a25$, respectively.

Nonetheless, the vibration control provided by the quarter ring was outstanding in all studied cases as can be seen in Figures 4.5.5 and 4.5.6 .

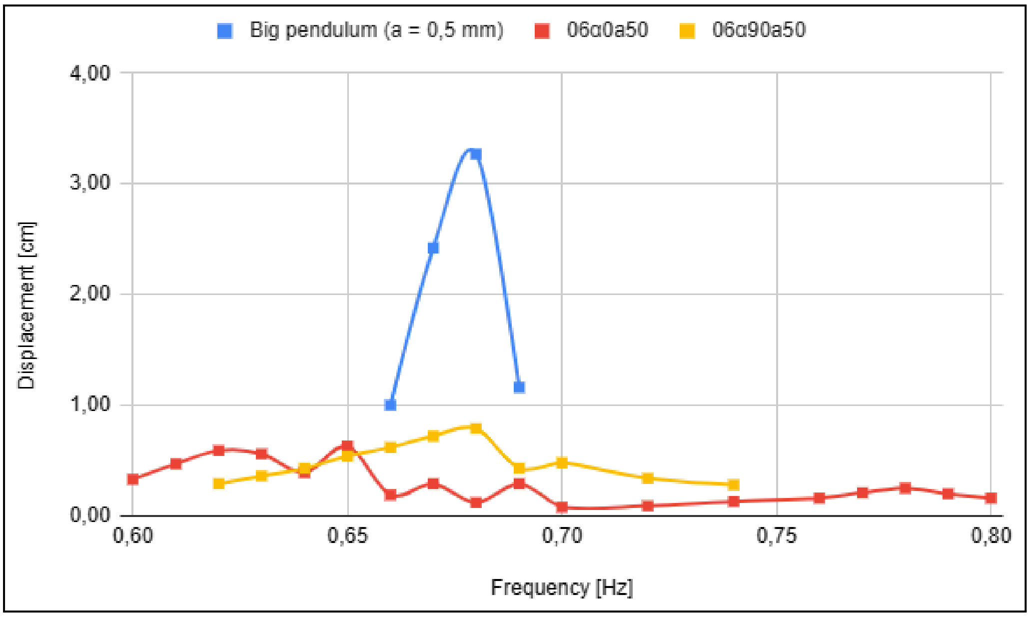

Figure 4.5.5 - Comparison between the big scale model with and without control for the higher base displacement amplitude.

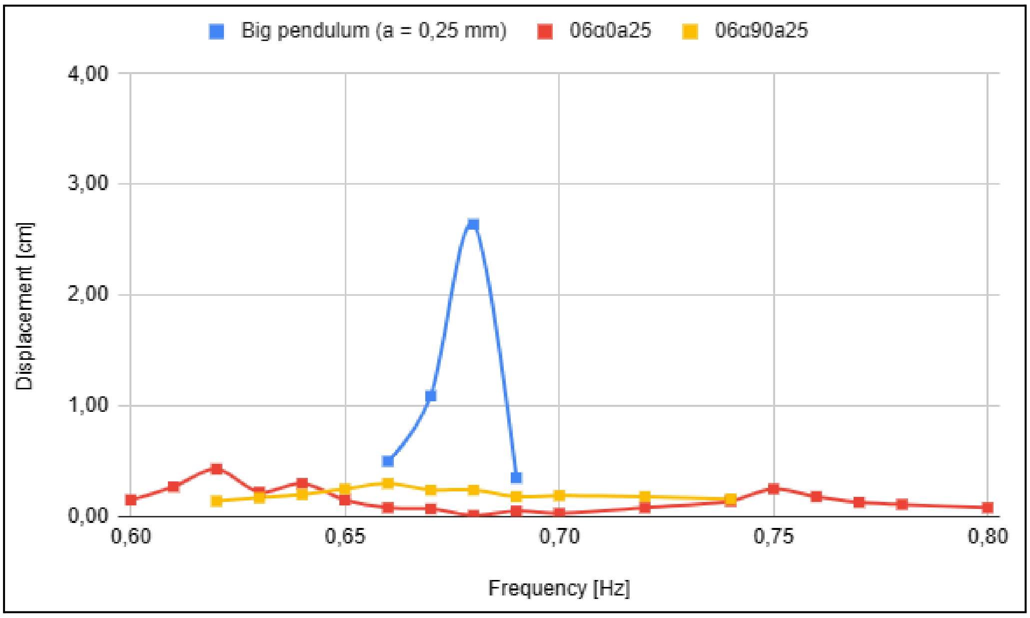

Figure 4.5.6 - Comparison between the big scale model with and without control for the lower base displacement amplitude.

…

5

CONCLUSIONS

The analytical methods utilised for the design of the rectangular TLD proved to be adequate for this purpose, in most cases, although the formula for the damping of liquid motion and, therefore, for the damping provided by the TLD to the system seemed inconsistent for the cases in which they were applied. This study further corroborates that the liquid depth ratio is an important parameter when designing a rectangular TLD.

The flowing of water inside the reservoir seemed to follow the path of least resistance, even when this would result in a movement that was not aligned with the excitation of the reservoir, namely in the cases where the reservoir was rotated.

The multiple peak frequency-response curves for the cases that had a rotated reservoir was unexpected and something that was not mentioned in any of the surveyed literature. This was also the case for the high variation in the behaviour of the water when studied in different frequencies, as the main concern deduced from the aforementioned literature seemed to be the height of the liquid inside the reservoir and its amplitude of displacement.

When dealing with the ring cell reservoir, it was demonstrated that the design methods utilised for rectangular TLD were also applicable, even though there was a small decrease in the performance of the TLD in those conditions. This also seems to be the case for the behaviour of the liquid inside the compartmentalised annular TLD, although the execution of a direct comparison with a MTLD composed of rectangular reservoirs was not possible.

The application of the MTLD in the form of the quarter ring TLD proved to be an adequate solution for relatively high displacement of the structure even when the central cell was not aligned with this excitation. The effectiveness of the analytical methods implemented is difficult to assess as most of the cells had the same behaviour and only two different configurations were studied.

As for the difference in behaviour due to the displacement amplitude, the collected data showed that the TLD has a worse performance the higher the displacement. Although, as mentioned beforehand, the difference in the resonance amplitudes in this study reached only 20% due to concerns about the integrity of the studied structure for higher amplitudes.

The study of TLD and its effects on the behaviour of structures is a vast topic, therefore, it must be said that further investigation in this area and its many nuances is still required.

REFERENCES AND BIBLIOGRAPHY

References

Abramson, H.N. (1966) *The Dynamics of Liquids in Moving Containers*. Urbana: University of Illinois, Web.

Bauer, H.F. (1960). *Theory of fluid oscillations in a circular cylindrical ring tank partially filled with liquid*. NASA TN-D-557.

Clough, R.W. & Penzien, J. (1975). *Dynamics of Structures*. McGraw-Hill: New York.

Fujino, Y.; Sun, L.M.; Pacheco, B.M. & Chaiseri, P. (1992). *Tuned Liquid Damper (TLD) for Suppressing Horizontal Motion of Structures*. Journal of Engineering Mechanics, v. 118, n. 10, p. 2017-2030.

Fujino, Y. & Sun, L.M. (1993). *Vibration Control by Multiple Tuned Liquid Dampers (MTLDs)*. Journal of Structural Engineering, v. 119, n. 12, p. 3482-3502

Ghaemmaghami, A.R.; Kianoush, R. & Mercan, O. (2016). *Numerical modeling of dynamic behavior of annular tuned liquid dampers for the application in wind towers under seismic loading*. Journal of Vibration and Control, v. 22, n.18, p. 3858–3876.

Grala, P. (2013). *Chaminés Industriais: Soluções para Atenuação de Vibrações Induzidas por Desprendimento de Vórtices*. Msc, Universidade Federal do Rio Grande do Sul.

Ibrahim, R.A.; Pilipchuk, V.N. & Ikeda, T. (2001). *Recent advances in liquid sloshing dynamics*. Applied Mechanics Reviews, v. 54, n.2, p. 133–199.

Jamal, O. (2015). *Numerical Investigation of a Tuned Liquid Damper Performance Attached to a Single Degree of Freedom Structure*. MSc, McMaster University.

Jorge, J.G.S. (2018). *Definition of a passive damping system (TMD) for an industrial steel chimney*. MSc, Instituto Superior Técnico

Konar, T. & Ghosh, A.D. (2022). *A review on various configurations of the passive tuned liquid damper*. Journal of Vibration and Control, v. 29, n. 9-10, p. 1945–1980.

Lepelletier, F. & Raichlen, T.G. (1988). *Nonlinear oscillations in rectangular tanks*. Journal of Engineering Mechanics, v. 114, n. 1, p. 1–23.

Miles, J.W. (1967). *Surface-wave damping in closed basins*. Proceedings of the Royal Society of London. Series A. Mathematical and Physical Sciences, v. 297, n. 1451, p. 459–475.

Moutinho, C. (1998). *Controlo passivo e activo de vibrações em pontes de peões*. MSc, Universidade do Porto.

Moutinho, C.; Cunha, A. & Caetano, E. (2010). *Implementation of Active and Passive Control Systems in Laboratorial and Real Structures*. Repositório Aberto da Universidade do Porto.

Novo, T.; Varum, H.; Teixeira-Dias, F.; Rodrigues, H.; Silva, M.F.; Costa A.C. & Guerreiro L. (2014). *Tuned liquid dampers simulation for earthquake response control of buildings*. Bulletin of Earthquake Engineering, vol. 12, p. 1007-1024.

Ramos, L.J.S.T. (2010). *Study and Simulation of the Synchronized Pedestrian Footstep Load and Passive Damping Solutions for Footbridges*. PhD, Universidade do Porto.

Soong, T.T. & Spencer Jr., B.F. (2002). *Supplemental energy dissipation: state-of-the-art and state-of-the-practice*. Engineering Structures, volume 24, issue 3, march of 2002, p. 243-259.

Sun, L.M. (1991). *Semi-Analytical Modelling of Tuned Liquid Damper (TLD) with Emphasis on Damping of Liquid Sloshing*. PhD, University of Tokyo.

Sun, L.M.; Fujino, Y.; Pacheco, B.M. & Chaiseri, P. (1995). *The Properties of Tuned Liquid Dampers Using a TMD Analogy*. Journal of Earthquake Engineering and Structural Dynamics, v. 24, p. 967-976

Warburton, G. B. & Ayorinde, E. O. (1980). *Optimum absorber parameters for simple systems*. International Journal of Earthquake Engineering and Structural Dynamics, n. 8, p.197-217.

Welt, F. (1988) *A study of notation dampers with application to wind-induced oscillations*. PhD, University of British Columbia.

Yue, H.; Chen, J. & Xu, Q (2018). *Sloshing characteristics of annular tuned liquid damper (ATLD) for applications in composite bushings.* Structural Control and Health Monitoring, v. 25, n. 8, e2184.

NP EN 1991-1-4:2010 Eurocode 1 – Actions on structure – Part 1-4: General actions – Wind actions. Instituto Português da Qualidade.

Bibliography

An, Y.; Wang, Z.; Ou, G.; et al. (2019). *Vibration mitigation of suspension bridge suspender cables using a ring-shaped tuned liquid damper*. Journal of Bridge Engineering, v. 24, n. 4, p. 1–12.

Corbi, O. (2006). *Experimental Investigation on Sloshing Water Dampers Attached to Rigid Blocks*, Proceedings of the 5th WSEAS International Conference on Applied Computer Science, pp. 682-687. Hangzhou, China.

Konar, T. & Ghosh, A.D. (2021). *Use of deep liquid-containing tanks as dynamic vibration absorbers for lateral vibration control of structures: A review*. Iranian Journal of Science and Technology, Transactions of Civil Engineering, v. 46, p. 753–769

Mondal, J.; Nimmala, H.; Abdulla, S. & Tafreshi, R. (2014). *Tuned Liquid Damper*. Proceedings of the 3rd International Conference on Mechanical Engineering and Mechatronics, paper n. 68. Prague, Czech Republic.

Other references

Duflot, P. & Moutinho, C. (2020). *Test Report - Tuned Liquid Damper*. Modalyse Engineering, Belgium.

Open House Slovenia: https://www.openhouseslovenia.org/objekt/termoelektrarna-toplarna-ljubljana/. Date of access: 14th of June 2023